Impaired bidirectional communication between interneurons and oligodendrocyte precursor cells affects cognitive behavior

Lipao Fang[1], Na Zhao[1], Laura C. Caudal[1], Renping Zhao[2], Ching-Hsin Lin[3], Hsin-Fang Chang[3], Nadine Hainz[4], Carola Meier[4], Bernhard Bettler[5], Wenhui Huang[1], Anja Scheller[1], Frank Kirchhoff[1,*], Xianshu Bai[1,*]

1. Molecular Physiology, CIPMM, University of Saarland, 66421 Homburg, Germany
2. Biophysics, CIPMM, University of Saarland, 66421 Homburg, Germany
3. Cellular Physiology, CIPMM, University of Saarland, 66421 Homburg, Germany
4. Department of Anatomy and Cell Biology, University of Saarland, 66421 Homburg, Germany
5. Department of Biomedicine, University of Basel, 4056 Basel, Switzerland

Correspondence to:

Prof. Dr. Frank Kirchhoff,
Molecular Physiology,
CIPMM, University of Saarland,
66421 Homburg, Germany
frank.kirchhoff@uks.eu

Dr. Xianshu Bai
Molecular Physiology,
CIPMM, University of Saarland,
66421 Homburg, Germany
xianshu.bai@uks.eu

Abstract

Cortical neural circuits are complex but very precise networks of balanced excitation and inhibition (E/I). Yet, the molecular and cellular mechanisms that form the E/I balance are just beginning to emerge. Here, using conditional $GABA_B$ receptor-deficient mice we identified a GABA/TNF-related cytokine (TNFSF12)-mediated bidirectional communication pathway between Parvalbumin-positive (PV^+) fast spiking interneurons and oligodendrocyte precursor cells (OPCs) that determines the density and function of interneurons in the developing medial prefrontal cortex (mPFC). Interruption of the GABAergic signaling to OPCs resulted in reduced myelination and hypoactivity of interneurons, strong changes of cortical network activities and impaired cognitive behavior. In conclusion, glial transmitter receptors are pivotal elements in finetuning distinct brain functions.

Introduction

The inhibition of cortical network activity is performed by interneurons that release the inhibitory transmitter γ-aminobutyric acid (GABA) which acts on ionotropic $GABA_A$ and metabotropic $GABA_B$ receptors [1, 2]. Alterations of interneuron cell density as well as concomitant changes of firing activity are often observed in several neuropsychiatric conditions [3-6]. In the mouse cortex, higher frequencies of spontaneous inhibitory postsynaptic currents (sIPSCs) were observed after increasing the interneuron density by transplantation of precursor cells [7]. Similarly, blocking of interneuron apoptosis caused a decrease of the excitation/inhibition (E/I) ratio [6, 8]. Interneuron density is a pivotal determinant of correct inhibitory circuits in the central nervous system (CNS). During development, a surplus of interneurons is generated that populates the cortical plate [9]. Subsequently, about 40 % of cortical inhibitory neurons are eliminated by programmed cell death during the first two

postnatal weeks [7]. One hypothesis links the apoptosis of supernumerary neurons with the onset of first neuron-neuron connections [10]. Only the neurons that receive sufficient neurotrophic signals from their target cells will survive [10, 11].

Oligodendrocyte precursor cells (OPCs) form synapses with interneurons as early as postnatal day (p) 4-5 [12]. Concomitantly, the incidence of interneuron apoptosis increases drastically after p5 and reaches its peak at p7 [7]. Right after, the interneuron-OPC connectivity accelerates till p10, which drives an immediate oligodendrocyte (OL) boom and subsequent interneuron myelination via OPC-$GABA_A$ and $GABA_B$ receptors [13-15]. Despite relatively short axons, myelination of cortical interneurons (mainly parvalbumin $(PV)^+$ fast-spiking interneurons, [16]) contributes significantly to the fine-tuning of local activity in the medial prefrontal cortex (mPFC) and cortex, ensuring proper performance of behavior [4, 17]. However, how the early communication between interneuron and OPC affect inhibitory network activity in the mPFC still remains unknown.

To assess the function of OPC $GABA_B$Rs for mPFC inhibition, we conditionally deleted the $GABA_B$ receptor subunit *gabbr1* selectively in OPCs at the end of the first postnatal week. By focusing on the medial prefrontal cortex (mPFC), we found that OPCs shape the inhibitory network by $GABA_B$ receptor and the cytokine tumor necrosis factor-like weak inducer of apoptosis (TWEAK) signaling pathways, thereby finetuning interneuron cell death and survival as well as its myelination onset. The functional and morphological changes of PV^+ interneurons observed in the adult mPFC of mutant mice generate a reduction of the inhibitory tone, which finally leads to impaired cognition and social behavior.

Results

$GABA_B$Rs of OPCs are required for oligodendrogenesis in the mPFC

To assess the function of $GABA_B$Rs for OPC-interneuron communication, we generated Tg*(NG2-CreER^{T2}):GABA$_{B1}$R$^{fl/fl}$* mice (Fig. 1a) to conditionally knockout (cKO) functional $GABA_B$R from OPCs and their progeny. We induced the cKO at postnatal day 7 and 8 (p7/8) before the onset oligodendrocyte formation at p10-11 [13]. When analyzed at the age of 9 weeks (w), about 80 % of OPCs (platelet-derived growth factor receptor α$^+$ (PDGFRα$^+$, Pα+))were found recombined (Pα$^+$tdT$^+$/Pα$^+$) in the medial prefrontal cortex (mPFC), based on tdTomato (tdT) gene expression (Fig. 1b, c).

To confirm and quantify the deletion of $GABA_B$R in OPCs, we performed Western blot analysis with OPCs purified by magnetic-activated cell sorting (MACs-OPCs). In cKO OPCs, $GABA_B$R expression was reduced by about 64 % compared with controls (ctl) (Fig. 1d). Considering the substantial purity of MACS-sorted OPCs (85 %, data not shown) and recombination efficiency (80 %), we concluded that a vast majority of $GABA_B$Rs had been ablated from OPCs.

Next, we focused on the oligodendrocyte lineage and evaluated the contribution of $GABA_B$Rs for OPC differentiation in the mPFC by immunostaining of PDGFRα and adenomatous polyposis coli clone 1 (CC1) (Fig. 1e), established markers for OPCs and oligodendrocytes, respectively. In the cKO mice, the density of OPCs (PDGFRα$^+$Olig2$^+$) did not change (Fig. 1f), while that of mature oligodendrocytes (CC1$^+$Olig2$^+$) was strongly reduced by 26 %(Fig. 1g), indicative of decreased OPC differentiation to oligodendrocytes (Fig. 1h). Notably, in the corpus callosum the densities of oligodendrocytes and OPCs, as well as their relative proportions did not differ between ctl and cKO mice (Fig.1 f-h, Extended Data Fig. 1). These data

suggest that OPC-$GABA_B$Rs are required for OPC differentiation in the grey matter mPFC, but not in the white matter corpus callosum.

We further analyzed structural aspects of myelination which is important for axonal conductivity, i.e. the lengths of nodes (the gaps between paired contactin-associated protein-positive ($Caspr^+$) segments) and paranodes (single $Caspr^+$ segments) by immunostaining (Fig. 1i). In cKO mPFC, the paranodal length was increased (Fig. 1j) while node length and density remained stable (Extended Data Fig. 2). In parallel, we observed a reduction of myelin basic protein (MBP) expression at the mRNA (Extended Data Fig. 2) and protein levels (Fig. 1k) in cKO mPFC, while the other myelin protein, proteolipid protein (PLP) mRNA levels were not changed (Extended Data Fig. 2). In the corpus callosum, however, myelination was unperturbed as indicated by unchanged paranode length (Extended Data Fig. 2), node density (Extended Data Fig. 2) and MBP expression (Fig. 1k). Therefore, our data show that $GABA_B$Rs of OPCs promote differentiation and myelination in the mPFC, but do not affect the corpus callosum.

Since OPCs continuously differentiate into oligodendrocytes [18-20], the cKO mice will also generate oligodendrocytes lacking $GABA_B$Rs. To selectively target only oligodendrocytes, we used Tg*(PLP-Cre^{ERT2}):GABA$_{B1}$R$^{fl/fl}$* mice (Extended Data Fig. 3) . The gene deletion was induced by tamoxifen injections at p7/8 or at 4w. At the age of 9w, we did not observe differences in the OPC and oligodendrocyte population between ctl and cKO mice (Extended Data Fig. 3), neither in the PFC nor in the corpus callosum (Extended Data Fig. 3).

In summary, our data strongly suggest that $GABA_B$R is specifically required for early OPC differentiation and subsequent myelination in the mPFC, but not in the corpus callosum.

$GABA_B$Rs of OPCs promote the myelination of interneurons in the mPFC

Since callosal axons are primarily excitatory [21] and axons of inhibitory interneurons are largely restricted to cortical areas of the same hemisphere (including mPFC, Fig.1l) (Extended Data Fig. 4), we hypothesized that the observed myelin deficits were restricted to interneurons. Required by their fast-spiking activity, parvalbumin $(PV)^+$ interneurons are the most abundantly myelinated interneurons [16, 22-24] of the cortex. These neurons are most prominent at the layer 4 and 5 with majority of their axons projecting to the layer 2/3 and 5 [25] (Fig. 1l, Extended Data Fig. 4). To evaluate their myelination, we performed PV and MBP double immunostaining (Fig. 1l-n) and analyzed the volume of myelin sheaths, by volume rendering of MBP immunolabel covering PV^+ axons at the cortical layers 2/3 of mPFC. Indeed, the volume of myelin sheaths wrapping PV neurons was reduced by 60 % in the cKO mPFC (Fig. 1n). However, the myelination of excitatory neurons (in the corpus callosum) was not affected as the g-ratio of myelinated axons and conduction velocity of compound action potential did not differ between ctl and cKO mice (Extended Data Fig. 2). Thus, we concluded that $GABA_BR$ of OPCs are preferentially involved in the myelination of inhibitory rather than excitatory neurons.

Postnatal deletion of $GABA_B$Rs in OPCs causes enhanced interneuron density in the adult, but with reduced GABA release

While investigating the interneuronal myelination, we recognized that early ablation of $GABA_BR$ in OPCs (at p7/8, Fig. 2a) was associated with a 20 % increase of interneuron density in the cortex as revealed by immunostaining for PV (Fig. 2b). However, in the mPFC this increase did not result in a concomitant increase of inhibitory input (Fig. 2c, d). In contrast, the frequency of spontaneous inhibitory postsynaptic currents (sIPSCs) of pyramidal neurons in the layer V of mPFC, where

interneurons are abundantly located, was reduced by 50 %, while the amplitude of sIPSCs remained unaffected in the mutant mPFC as well as the firing rate and amplitude of excitatory postsynaptic currents (EPSCs).

Since neuronal activity can regulate myelination [22, 26], we asked whether the reduced inhibitory firing rate contributed to the observed molecular and structural changes of the myelin at interneuronal axons in the mutant mPFC. For that purpose, we further analyzed the cKO mPFC of p10 mice (Fig. 2e) at the onset of myelination and when interneuron-OPC communication peaks [13]. After induction of the cKO at p7/8, we assessed the density of the vesicular GABA transporter (vGAT) close to OPC surfaces as a quantitative readout of inhibitory presynaptic terminals by combined vGAT and PDGFRα immunostaining [27] (Fig. 2f-i, Extended Data Fig. 5). We classified the vGAT puncta into two subgroups based on the distance between vGAT staining and OPC surface: '<20 nm' as vesicles targeting on postsynaptic OPCs (magenta), and '>20 nm' as vesicles targeting on other cells (grey), assuming a width of about 20 nm for the synaptic cleft [28]. And indeed, already at p10, i.e. only 3 days after the first tamoxifen injection, the density and the volume of vGAT immunopuncta were reduced were reduced to 75 % and 80 % in the cKO mPFC (Fig. 2f-i, Extended Data Fig. 5), including a smaller volume of vGAT (Fig. 2h) and less puncta (Fig. 2i) at the OPC surface in cKO mPFC, which can explain the attenuated firing rate of the interneurons in the adult. These results indicate that interneurons exhibit lower activity and transmit less GABAergic signals to OPCs in the cKO mPFC.

To test whether the reduced inhibitory tone affecting OPC differentiation specifically correlates with the onset of myelination, we compared the OPC and oligodendrocyte populations at p10 and p14 (Fig. 2j-m, Extended Data Fig. 6). At p10, the densities of OPC and oligodendrocyte populations were still comparable in the cKO mPFC to control mPFC, although the interneurons already expressed less vGAT (Fig. 2f-h). However, at p14, the differentiation and cell numbers of oligodendrocytes dropped

strongly in the mutant mPFC (Fig. 2l, Extended Data Fig. 6), as did the MBP expression (Fig. 2m). Again, in the corpus callosum, OPC and oligodendrocyte population were not affected by the deletion of $GABA_BRs$ (Extended Data Fig. 1).

When we induced $GABA_BR$ deletion in the young adult mice at the age of 4 weeks, both in the mPFC and corpus callosum, the density of oligodendrocyte as well as the MBP expression were not affected in the cKO mice (Extended Data Fig. 7).

In summary, our data strongly suggest that during early development of the mPFC deletion of $GABA_BR$ in OPCs affects the inhibitory tone of interneurons, feeding back onto OPC differentiation and interneuron myelination.

OPCs induce interneuron apoptosis via $GABA_BR$-TWEAK signaling

As we had seen a surplus of interneurons in the mutant mPFC which could explain the abnormal neuronal activity [8, 29], we tested whether the interneuron numbers would be accurately controlled by programmed cell death early during development. After induction of $GABA_BR$ in OPCs at p7/8, the extent of interneuron apoptosis was determined at p10 and p14 by immunostaining for PV and cleaved caspase-3 (CC-3, Extended Data Fig. 8), a well-established marker for apoptosis. As expected by the earlier experiments, we found 50 % reduction of $PV^+/CC\text{-}3^+$ interneurons at p10 suggestive of strongly reduced apoptosis of PV^+ interneurons in the mutant mPFC (Extended Data Fig. 8). Obviously, OPCs receive GABAergic input through $GABA_BR$ and send back pro-apoptotic signals to interneurons.

To confirm the selective cell death of interneurons, we induced the cKO as early as p1 and p2 and compared the apoptosis of inhibitory neurons with that of excitatory ones at p5 and p7 (Fig. 3a). Interneuron apoptosis persists from p1 till p15 with a peak at p7 [7], while the time window for excitatory neuron apoptosis is rather narrow, between p2-5 [30]. Apoptosis of total interneurons ($GAD67^+CC\text{-}3^+$) as well as PV

interneurons ($PV^+CC\text{-}3^+$ left panel in Fig. 3b) was significantly reduced in cKO mPFC at p5 and p7 (Fig. 3c), while that of the excitatory neurons ($CTIP^+CC\text{-}3^+$, right panel in Fig. 3b; $TBR1^+CC\text{-}3^+$) did not change at both time points (Fig. 3c, Extended Data Fig. 9). Therefore, we concluded that OPCs send pro-apoptotic signals back to interneurons at the early postnatal weeks.

To molecularly identify the critical apoptotic factor released by OPCs, we first tested the expression levels of several peptides which had been associated with cell survival or cell death in ctl and cKO mPFC (Extended Data Fig. 10). Gene deletion was induced at p1/2, and mPFC was collected at p7, the peak of interneuron apoptosis (Extended Data Fig. 10). We found only the expression of the cytokine tumor necrosis factor-like weak inducer of apoptosis (TWEAK, also known as Apo3l or TNF superfamily member 12, TNFSF12) to be diminished about 30 % in cKO mPFC (Fig. 3d, Extended Data Fig. 10). TWEAK induces an apoptotic cell death after binding to its cognate TWEAK receptor (TWEAKR; TNF Receptor Superfamily Member 12A, TNFRSF12A; also known as FN14) [31]. Subsequently, we tested MACS-sorted OPCs (collected from cKO and ctl cortices at p7) (Fig. 3d) as well as Oli-neu cells (an OPC cell line) treated with $GABA_BR$ antagonist CGP 55845 for TWEAK. Also here, we observed TWEAK downregulation (Extended Data Fig. 10). Three independent experiments, including genetic deletion or pharmacological block of OPC $GABA_BR$ decreased TWEAK expression (Fig. 3d, Extended Data Fig. 10).

To confirm that OPC-derived TWEAK can indeed induce neuronal apoptosis, we treated primary cortical neurons with conditioned medium obtained from OPC Oli-neu cultures (Fig. 3e). A selective TWEAKR antagonist, L524-0366 was added to the conditioned medium at 20 µM to block the binding of TWEAK on interneurons (Fig. 3e, f). While the conditioned medium from the OPC cell line increased interneuron apoptosis (Fig. 3g, h), co-treatment with the TWEAKR antagonist

prevented the cell death. These results further substantiate that OPCs induces interneuron apoptosis via TWEAK secretion.

In summary, our results demonstrate that OPCs induce interneuron apoptosis by releasing TWEAK upon $GABA_BR$ activation. Blocking this pathway prevents the apoptosis of interneurons. The concomitant dysregulation of interneuron density results in a reduced inhibitory GABAergic tone and altered myelination in the mPFC.

Interrupted OPC-interneuron communication after $GABA_BR$ loss in OPCs during development generates cognitive impairment in adulthood

The mPFC is responsible for cognitive processes and their regulatory finetuning is guaranteed by the E/I balance [32]. To test whether the selectively reduced interneuron apoptosis and the associated structural myelin alterations can generate defects in neural circuits and cognition, we further performed *in vivo* investigations using electrophysiology and behavioral analysis in 9w old animals after gene ablation was induced at P7/8 (Fig. 4a).

The patch-clamp recordings described above had revealed a reduced firing rate of interneurons suggesting an imbalance of E/I in the mutant mPFC (Fig. 2c, d). Impaired cortical network activity of the mutant mice was also detected in electroencephalographical (EEG) recordings. The power of the gamma wave, especially the lower gamma wave band (30-50 Hz) was slightly, but significantly decreased by about 10% in cKO mice (Fig. 4b).

To evaluate the impact of circuit dysregulation in the mutant mPFC for the living animal, we challenged mice for their cognitive performance employing tasks of social cognitive behavior which had been associated with proper mPFC function, i.e. social novelty and new object recognition [33]. In addition, nest building behavior is often introduced as a gauge of general well-being of the mice and also being an early sign

of cognition decline [34]. We observed that the mutant mice built significantly poorer nests with less than half score of the control animal nests, indicating putative cognition deficits of the mutant mice (Fig. 4c). The three-chamber test was used to assess social cognition by analyzing mice for a form of general sociability and their interest in social novelty (Fig. 4d). First, the three-chamber test was used to monitor general social behavior, i.e. preference of other mice over objects. Both, ctl and cKO mice exhibited more interest in the mouse rather than the object during the first test phase, indicating no disorder in sociability of the mutant mice (Fig. 4e, Extended Data Fig. 11). At the second phase, a social novelty preference was assessed. Control animals investigated the unfamiliar mouse more than the familiar one, while the cKO mice exhibited no novel social preference as they spent similar time in both chambers (Fig. 4f, Extended Data Fig. 11). Employing a new object recognition test (Fig. 4g), we again observed the cognition defect of cKO mice. Control animals were able to distinguish the new object replaced after a 40 min break from the habituation, while the cKO mice showed similar interest to both of the old and new objects (right panel in Fig. 4g-i). Open field test showed that the motor activity of the cKO mice (in terms of the speed and total distance) was not affected (Fig. 4j-l).

Hence, we conclude that $GABA_BRs$ of OPCs are essential for cognition by modifying inhibitory circuits in the mPFC.

Discussion

A balance of excitation and inhibition (E/I) in the medial prefrontal cortex (mPFC) is of key importance for mammalian cognition. Establishing correct cell densities and subsequent myelination have been identified as pivotal elements during CNS development [6, 17]. This has been well documented for fast-spiking parvalbumin-positive (PV^+) interneurons. Here, we highlight OPCs as indispensable regulators of interneuron population and myelination in the mPFC by providing a molecular explanation and demonstrating how impaired bidirectional OPC-interneuron signaling affects social cognitive behavior. OPCs at the first two postnatal weeks release TWEAK to regulate interneuron apoptosis. Genetic ablation of $GABA_BR$ in OPCs at the first postnatal week promoted interneuron survival. However, these neurons displayed hypoactivity, less contacts with OPCs during development and deteriorated myelin structures in the adulthood. Notably, these mutant mice exhibited severe cognitive defects in their social behavior.

During development, large populations of immature interneurons invade the cortex where their cell density is adjusted by programmed cell death [9, 10]. For assuring their survival, these neurons form connections with adjacent cells and receive retrograde signals from their targets [10, 11]. Interneuron apoptosis drastically increases at p7 [7], shortly after formation of interneuron-OPC synapses at p4-5 [12]. Based on this established knowledge, we hypothesized that OPCs could exert an apoptotic impact to their presynaptic partners. Indeed, our data provide strong evidence that, starting from postnatal day 5 on, OPCs elicit an apoptotic cascade of adjacent interneurons to adjust their density. In OPCs, the regulatory process employs a $GABA_BR$-TWEAK signaling pathway. TWEAK, TNF super family member 12 (TNFSF12), is TNF-like weak apoptotic factor. Membrane-bound and cleaved isoforms of TWEAK are both able to induce cell apoptosis by binding to the TWEAK receptor (TWEAKR, also known as FN14) on the neuronal side [31, 35, 36]. According to our data $GABA_BR$-

TWEAK signaling preferentially affects interneurons, suggesting this ‘kill me’ signal acting highly localized. Indeed, TWEAK is specifically recruited to synapses where TWEAKRs are expressed [37]. OPCs directly sense GABAergic signals at their interneuron-OPC synapse. Subsequent signaling triggers TWEAK expression and translocation to the OPC surface, where it could directly bind interneuronal TWEAKRs. Alternatively, the TWEAK ectodomain could be proteolytically cleaved and act as a soluble factor. However, this scenario could also happen at soma-somatic contact sites between OPCs and interneurons [38, 39]. The regulatory impact appears to be highly specific since the OPC-induced interneuron apoptosis was restricted to the first two postnatal weeks, a well-established time window of interneuron apoptosis [7, 30]. This also explains why the cKO induction at the age of 4w did not impact OPC differentiation and myelination, although $GABA_BR$ expression peaks in OPCs at 4w (data not shown). Please note, instead of a gradual decline, we found a slight increase of PV^+CC3^+ cells at p14 compared to p10, probably due to the age-dependent increase of PV expression described for fast spiking interneurons [40]. During the same time period of interneuronal apoptosis a substantial portion of OPCs arriving in the cortex are eliminated as well [41]. This first wave of OPCs share the same cellular origin with a 60 % majority of interneurons, i.e. $Nkx2.1^+$ precursors from the medial ganglionic eminence (MGE) and the embryonic preoptic area (ePOA) [9, 41]. However, whether a causal link exists between common origin and $GABA_BR$/TWEAK-mediated interneuron-OPC signaling requires further analysis.

Differentiation of oligodendrocytes and subsequent myelination are strongly affected by neuronal activity [22, 26, 42]. Indeed, when we induced $GABA_BR$ loss at p7, we observed a suppression of the inhibitory tone in the mPFC early in development (p10; attenuated expression of vGAT in interneurons and less vGAT puncta on the surface of OPCs), before a change in oligodendrocyte density could be detected at p14. Concomitantly, the oligodendrocytes formed less myelin around the interneuronal

axons and altered paranodal structures in the adult mPFC which are essential for precise action potential propagation. The morphological deterioration was only observed in the mPFC, but not in the corpus callosum composed axons of excitatory neurons only [21]. In line with these neuron-type specific observations, the qRT-PCR results indicated reduced levels of MBP, but not PLP mRNA expression in the mutant mPFC, both at p14 and 9w of age. Axons of interneurons and excitatory neurons are different in respect to the protein content of their myelin sheaths. MBP is preferentially expressed in the myelin of inhibitory axons, while PLP is more prominent in excitatory axons PLP [16].

An early loss of the $GABA_AR$ γ2 subunit in OPCs reduced the firing rate of presynaptic PV^+ interneurons and caused a similar myelin defect of longer nodal structures in PV^+ neurons [4], the initially very different signal pathways of both, $GABA_AR$ and $GABA_BR$, have to merge to affect myelin gene expression and OPC-axon contacts similarly. The $GABA_AR$ signaling between interneurons and OPCs is relatively well established [4, 15, 43, 44]. E.g., the γ2 subunit of $GABA_AR$ contributes to the maintenance of the OPC, but has no impact on oligodendrocyte formation [15]. However, the role of $GABA_BRs$ for OPC differentiation is complex. We observed that $GABA_BR$ was essential for oligodendrogenesis at the early development but not at later stages. Similary, an *in vitro* study showed that activation of $GABA_BR$ by the selective agonist baclofen could stimulate the differentiation of cortical OPCs prepared from p0-2 pups [14]. Since OPCs are heterogeneous with age [45], $GABA_BR$ of OPCs could contribute to the developmental diversity.

Obviously, the GABAergic signaling of OPCs plays pivotal roles for the myelination of interneurons, which ensures precise finetuning of the local neural circuitry [46]. As seen in chandelier cells [6], excessive number of interneurons in the OPC-$GABA_BR$ cKO mice exhibited suppressed activity, and reduced myelination in the mPFC. All these physiological and morphological abnormalities certainly contributed to cognition

impairment. A proper E/I ratio in the prefrontal cortex, especially early E/I balance in mPFC, is extremely important for social cognition [32, 47]. When the pyramidal neuron activity was enhanced in the mPFC at early p7-11 caused a severe cognitive dysfunction in the adulthood [47]. In addition, despite relatively short axons, myelination of cortical interneurons (mainly PV^+ neurons [16]) contributes significantly to the finetuning of local activity in the mPFC and cortex, insuring proper behavior performance [4, 6, 17].

In conclusion, our study demonstrates that OPCs regulate inhibition in the mPFC via $GABA_BR$/TWEAK signaling. During development, OPCs determine the density of interneurons by adjusting their apoptosis. Subsequently, correct myelination of interneurons, as an essential component of the network activity in the mPFC, determines the cognition and social behavior.

References

1. Douglas, R.J. & Martin, K.A. Inhibition in cortical circuits. *Curr Biol* **19**, R398-402 (2009).

2. Bai, X., Kirchhoff, F. & Scheller, A. Oligodendroglial GABAergic Signaling: More Than Inhibition! *Neurosci Bull* (2021).

3. Marín, O. Interneuron dysfunction in psychiatric disorders. *Nat Rev Neurosci* **13**, 107-120 (2012).

4. Benamer, N., Vidal, M., Balia, M. & Angulo, M.C. Myelination of parvalbumin interneurons shapes the function of cortical sensory inhibitory circuits. *Nat Commun* **11**, 5151 (2020).

5. Ferguson, B.R. & Gao, W.J. PV Interneurons: Critical Regulators of E/I Balance for Prefrontal Cortex-Dependent Behavior and Psychiatric Disorders. *Front Neural Circuits* **12**, 37 (2018).

6. Wang, B.S.*, et al.* Retinal and Callosal Activity-Dependent Chandelier Cell Elimination Shapes Binocularity in Primary Visual Cortex. *Neuron* **109**, 502-515.e507 (2021).

7. Southwell, D.G.*, et al.* Intrinsically determined cell death of developing cortical interneurons. *Nature* **491**, 109-113 (2012).

8. Orduz, D.*, et al.* Developmental cell death regulates lineage-related interneuron-oligodendroglia functional clusters and oligodendrocyte homeostasis. *Nat Commun* **10**, 4249 (2019).

9. Lim, L., Mi, D., Llorca, A. & Marín, O. Development and Functional Diversification of Cortical Interneurons. *Neuron* **100**, 294-313 (2018).

10. Davies, A.M. Regulation of neuronal survival and death by extracellular signals during development. *EMBO J* **22**, 2537-2545 (2003).

11. Oppenheim, R.W. Cell death during development of the nervous system. *Annu Rev Neurosci* **14**, 453-501 (1991).

397 12. Vélez-Fort, M., Maldonado, P.P., Butt, A.M., Audinat, E. & Angulo, M.C. Postnatal
398 switch from synaptic to extrasynaptic transmission between interneurons and NG2 cells. *J*
399 *Neurosci* **30**, 6921-6929 (2010).
400 13. Orduz, D.*, et al.* Interneurons and oligodendrocyte progenitors form a structured
401 synaptic network in the developing neocortex. *Elife* **4** (2015).
402 14. Serrano-Regal, M.P.*, et al.* Oligodendrocyte Differentiation and Myelination Is
403 Potentiated via GABA. *Neuroscience* **439**, 163-180 (2020).
404 15. Balia, M., Benamer, N. & Angulo, M.C. A specific GABAergic synapse onto
405 oligodendrocyte precursors does not regulate cortical oligodendrogenesis. *Glia* **65**, 1821-
406 1832 (2017).
407 16. Micheva, K.D.*, et al.* A large fraction of neocortical myelin ensheathes axons of local
408 inhibitory neurons. *Elife* **5** (2016).
409 17. Maas, D.A.*, et al.* Interneuron hypomyelination is associated with cognitive
410 inflexibility in a rat model of schizophrenia. *Nat Commun* **11**, 2329 (2020).
411 18. Huang, W.*, et al.* Novel NG2-CreERT2 knock-in mice demonstrate heterogeneous
412 differentiation potential of NG2 glia during development. *Glia* **62**, 896-913 (2014).
413 19. Kang, S.H., Fukaya, M., Yang, J.K., Rothstein, J.D. & Bergles, D.E. NG2+ CNS glial
414 progenitors remain committed to the oligodendrocyte lineage in postnatal life and following
415 neurodegeneration. *Neuron* **68**, 668-681 (2010).
416 20. Zhu, X.*, et al.* Age-dependent fate and lineage restriction of single NG2 cells.
417 *Development* **138**, 745-753 (2011).
418 21. Fame, R.M., MacDonald, J.L. & Macklis, J.D. Development, specification, and
419 diversity of callosal projection neurons. *Trends Neurosci* **34**, 41-50 (2011).
420 22. Stedehouder, J.*, et al.* Fast-spiking Parvalbumin Interneurons are Frequently
421 Myelinated in the Cerebral Cortex of Mice and Humans. *Cereb Cortex* **27**, 5001-5013 (2017).

422 23. Stedehouder, J., *et al.* Local axonal morphology guides the topography of
423 interneuron myelination in mouse and human neocortex. *Elife* **8** (2019).
424 24. Zonouzi, M., *et al.* Individual Oligodendrocytes Show Bias for Inhibitory Axons in the
425 Neocortex. *Cell Rep* **27**, 2799-2808.e2793 (2019).
426 25. Scala, F., *et al.* Layer 4 of mouse neocortex differs in cell types and circuit
427 organization between sensory areas. *Nat Commun* **10**, 4174 (2019).
428 26. Mitew, S., *et al.* Pharmacogenetic stimulation of neuronal activity increases
429 myelination in an axon-specific manner. *Nat Commun* **9**, 306 (2018).
430 27. Chaudhry, F.A., *et al.* The vesicular GABA transporter, VGAT, localizes to synaptic
431 vesicles in sets of glycinergic as well as GABAergic neurons. *J Neurosci* **18**, 9733-9750 (1998).
432 28. Dani, A., Huang, B., Bergan, J., Dulac, C. & Zhuang, X. Superresolution imaging of
433 chemical synapses in the brain. *Neuron* **68**, 843-856 (2010).
434 29. Fang, W.Q., *et al.* Overproduction of upper-layer neurons in the neocortex leads to
435 autism-like features in mice. *Cell Rep* **9**, 1635-1643 (2014).
436 30. Wong, F.K., *et al.* Pyramidal cell regulation of interneuron survival sculpts cortical
437 networks. *Nature* **557**, 668-673 (2018).
438 31. Chicheportiche, Y., *et al.* TWEAK, a new secreted ligand in the tumor necrosis factor
439 family that weakly induces apoptosis. *J Biol Chem* **272**, 32401-32410 (1997).
440 32. Grossmann, T. The role of medial prefrontal cortex in early social cognition. *Front*
441 *Hum Neurosci* **7**, 340 (2013).
442 33. Bicks, L.K., Koike, H., Akbarian, S. & Morishita, H. Prefrontal Cortex and Social
443 Cognition in Mouse and Man. *Front Psychol* **6**, 1805 (2015).
444 34. Neely, C.L.C., Pedemonte, K.A., Boggs, K.N. & Flinn, J.M. Nest Building Behavior as an
445 Early Indicator of Behavioral Deficits in Mice. *J Vis Exp* (2019).
446 35. Winkles, J.A. The TWEAK-Fn14 cytokine-receptor axis: discovery, biology and
447 therapeutic targeting. *Nat Rev Drug Discov* **7**, 411-425 (2008).

448 36. Brown, S.A., Ghosh, A. & Winkles, J.A. Full-length, membrane-anchored TWEAK can
449 function as a juxtacrine signaling molecule and activate the NF-kappaB pathway. *J Biol Chem*
450 **285**, 17432-17441 (2010).
451 37. Cheadle, L.*, et al.* Sensory Experience Engages Microglia to Shape Neural
452 Connectivity through a Non-Phagocytic Mechanism. *Neuron* **108**, 451-468.e459 (2020).
453 38. Mangin, J.M., Kunze, A., Chittajallu, R. & Gallo, V. Satellite NG2 progenitor cells share
454 common glutamatergic inputs with associated interneurons in the mouse dentate gyrus. *J*
455 *Neurosci* **28**, 7610-7623 (2008).
456 39. Boulanger, J.J. & Messier, C. Oligodendrocyte progenitor cells are paired with GABA
457 neurons in the mouse dorsal cortex: Unbiased stereological analysis. *Neuroscience* **362**, 127-
458 140 (2017).
459 40. Larsen, R., Proue, A., Scott, E.P., Christiansen, M. & Nakagawa, Y. The Thalamus
460 Regulates Retinoic Acid Signaling and Development of Parvalbumin Interneurons in
461 Postnatal Mouse Prefrontal Cortex. *eNeuro* **6** (2019).
462 41. Kessaris, N.*, et al.* Competing waves of oligodendrocytes in the forebrain and
463 postnatal elimination of an embryonic lineage. *Nat Neurosci* **9**, 173-179 (2006).
464 42. Nagy, B., Hovhannisyan, A., Barzan, R., Chen, T.J. & Kukley, M. Different patterns of
465 neuronal activity trigger distinct responses of oligodendrocyte precursor cells in the corpus
466 callosum. *PLoS Biol* **15**, e2001993 (2017).
467 43. Balia, M.*, et al.* Postnatal down-regulation of the GABAA receptor γ2 subunit in
468 neocortical NG2 cells accompanies synaptic-to-extrasynaptic switch in the GABAergic
469 transmission mode. *Cereb Cortex* **25**, 1114-1123 (2015).
470 44. Passlick, S.*, et al.* Expression of the γ2-subunit distinguishes synaptic and
471 extrasynaptic GABA(A) receptors in NG2 cells of the hippocampus. *J Neurosci* **33**, 12030-
472 12040 (2013).

45. Spitzer, S.O., *et al.* Oligodendrocyte Progenitor Cells Become Regionally Diverse and Heterogeneous with Age. *Neuron* **101**, 459-471.e455 (2019).

46. Arancibia-Cárcamo, I.L., *et al.* Node of Ranvier length as a potential regulator of myelinated axon conduction speed. *Elife* **6** (2017).

47. Bitzenhofer, S.H., Pöpplau, J.A., Chini, M., Marquardt, A. & Hanganu-Opatz, I.L. A transient developmental increase in prefrontal activity alters network maturation and causes cognitive dysfunction in adult mice. *Neuron* (2021).

Acknowledgement

We thank Daniel Schauenburg for excellent animal husbandry and Frank Rhode, Alexander Grissmer and Samantha Bechet for experimental assistance. We are also grateful to Prof. Jaqueline Trotter (University of Mainz, Mainz, Germany) for providing the Oli-neu cell line and Prof. Leda Dimou (University of Ulm, Ulm, Germany) for sharing MACs sorting protocols of OPCs. This work was supported by grants from the Deutsche Forschungsgemeinschaft (SPP 1757, SFB 894 to FK; FOR2289 to AS, FK, SPP1757 Young Investigator grant to XB), EraNet-Neuron BrIE to FK and HOMFORexzellent2017 program to XB.

Author contributions

XB initiated the project. LF, XB, NZ, LC, NH, CL and AS performed experiments. LF, XB, NZ, LC and RZ analyzed data. BB, WH. HC and CM provided materials. XB and FK designed and supervised the study and wrote the manuscript with comments of the other authors.

Competing interests

The authors declare no competing interests.

Figure legend

Figure 1. Ablation of $GABA_BRs$ in OPCs attenuates oligodendrocyte differentiation and myelination of interneurons in the medial prefrontal cortex. ***a***, Genetic strategy and experimental schedule. ***b***, Exemplary image of prefrontal cortex in coronal section stained with PDGFRα. tdTomato$^+$ (tdT$^+$) cells indicate recombined cells. ***b_1***, ***b_2***, magnified images of ctl and cKO medial prefrontal cortex (mPFC, highlighted in ***b***) stained with PDGFRα and tdTomato expression. ***c,*** Recombination efficiency of OPCs in ctl and cKO mPFC. (*ctl=4, cKO=5, unpaired t-test*). ***d,*** Western blot analysis of $GABA_BR$ subunit 1 in MACs sorted OPCs from cortex shows reduction of $GABA_{B1}R$ expression in cKO OPCs. (*ctl=3, cKO=3, unpaired t-test*). ***e,*** Exemplary images of Olig2 (oligodendrocyte lineage), PDGFRα (OPCs) and CC1 (oligodendrocyte) immunostaining in adult ctl and cKO mPFC. ***f, g,*** Quantification of OPC and oligodendrocyte cell densities in mPFC and corpus callosum (cc). (mPFC: *ctl=7, cKO=8, cc: ctl=4, cKO=4, multiple t-tests)*. ***h,*** Quantification of the oligodendrocyte proportion among the total lineage (mPFC: *ctl=4, cKO=4;* cc: *ctl=3, cKO=6, multiple t-tests)*. ***i,*** Immunostaining of Caspr and MBP in ctl and cKO mPFC. ***j,*** Quantitative analysis of paranode length in mPFC (*ctl=4, cKO=4, multiple t-tests*). ***k,*** Western blot analysis of MBP expression in mPFC and cc. (*ctl=4, cKO=3, multiple t-tests*). ***l,*** Overview of coronal brain slices immunostained with parvalbumin (PV) and MBP shows abundant PV$^+$ neurons are myelinated in mPFC. ***m***, 3D reconstruction of myelinated PV$^+$ axons in ctl and cKO mPFC using Imaris software. ***n***, Relative volume of MBP$^+$ myelin sheats wrapping PV$^+$ axons (*normalized to ctl). (ctl=3, cKO=3, unpaired t-test*).

Figure 2. In OPC-$GABA_BR$ cKO mice impaired control of interneuronal density and firing rate reduces oligodendrocyte differentiation and myelin gene expression at the onset of myelination. ***a,*** Experimental schedule for ***b-d***. ***b***,

Immonostaining (left) and quantification (right) of PV^+ neurons in the mPFC at the age of 9 weeks (*ctl=5, cK=9, unpaired t-test*). ***c,*** Exemplary traces of sIPSCs and sEPSCs recorded at the layer V of mPFC. ***d,*** Quantification of frequency and amplitude of sIPSC and sEPSC *(sIPSC: ctl=15 cells from 4 mice, cKO=15 cells from 5 mice; sEPSC: ctl=26 cells from 4 mice, cKO=21 cells from 5 mice, Mann Whitney test).* ***e,*** Experimental schedule for ***f-m***. ***f,*** 3D reconstruction of OPCs and vGAT by PDGFRα and vGAT immunostaining in ctl and cKO mPFC at p10 using Imaris software. vGAT was classified into two subgroups: magenta indicates vGATs which have < 20nm distance from OPC surface; grey vGATs have > 20nm from OPC surface. ***g, h***, Density (***g***) and volume (***h***) of vGAT in ctl and cKO mPFC. (*ctl=4, cKO=4; multiple t-tests*). ***i,*** Quantification of synaptic vGAT (< 20nm) density per μm^2 of OPC surface. *(ctl=4, cKO=4, unpaired t-test*). ***j,*** Immunostaining of OPCs and oligodendrocytes with PDGFRα, Olig2 and CC1 in p14 mPFC. ***k, l***, Density of OPCs (***k***) and oligodendrocytes (***l***) in ctl and cKO mPFC at p10 and p14. (*p10 and p14: ctl=5, cKO=4; multiple t-tests*). ***m,*** Quantitative analysis of MBP mRNA level in ctl and cKO mPFC at p14. (*ctl=4, cKO=4, unpaired t-test)*.

Figure 3. During early CNS development the apoptosis of supernumerous interneurons is mitigated upon impaired release of TWEAK from $GABA_BR$-deficient OPC. ***a,*** Scheme of experimental plan. ***b,*** Representative images of excitatory (CTIP) and inhibitory (PV^+) neurons co-stained with apoptotic marker CC-3 in p5 and p7 mPFC. ***c,*** Quantification of apoptotic neurons ($CC\text{-}3^+$) co-expressing interneuron marker GAD67 and PV or excitatory neuronal marker CTIP and TBR1. *(GAD67: p5-ctl=3, p5-cKO=4; p7-ctl=3, p7-cKO=5) (PV: p5-ctl=5, p5-cKO=3; p7-ctl=3, p7-cKO=5) (CTIP: p5-ctl=7, p5-cKO=4; p7-ctl=9, p7-cKO=3) (TBR1: p5-ctl=4, p5-cKO=4; p7-ctl=4, p7-cKO=4) (multiple t-tests)*. ***d,*** Relative mRNA level of TWEAK in the mPFC and MACs-OPCs from ctl and cKO mice *(tissue-ctl=4, tissue-cKO=6; MACs-ctl=4, MACs-cKO=3; multiple t-test).* ***e,*** Experimental design for *in vitro* studies.

f, Immunolabeling of TWEAK receptor on 14 DIV PV^+ interneurons. ***g,*** Immunostaining of apoptotic primary PV^+ neurons treated with conditional medium of Oli-neu cells co-treated with or without TWEAKR antagonist L524-0366 (20 µM). ***h,*** Percentage of apoptotic PV^+ neurons among total PV^+ neurons after the treatments *(n=3 independent experiments, one-way ANOVA, multiple comparison)*.

Figure 4. In OPC-$GABA_BR$ cKO mice perturbed electrical activity translates into deficits of social behavior. ***a,*** Scheme of experimental plan. ***b,*** Representative diagram of lower gamma band acquired by ECoG recordings. Violin plot shows decreased gamma oscillation in the cKO mouse brain. (*ctl=24 from 4 mice, cKO=24 from 4 mice, unpaired t-test*). ***c,*** Impaired nest building ability of mutant mice. (*ctl=9, cKO=10, Mann Whitney test*). ***d***, Scheme of three-chamber behavior test. ***e,*** Quantification of the sniffing time with mouse (***e***) or with unfamiliar mouse (***f***) among total sniffing time (*ctl=9, cKO=9, unpaired t-tests*). ***g,*** Scheme of new object recognition test. ***h,*** Assessment of object preference *(ctl=10, cKO=10)*. ***i,*** Percentage of sniffing time with new object among total sniffing time. *(ctl=10, cKO=10, upaired t-test*). ***j,*** Representative trajectory charts of the animals during the open field test. ***k, l,*** Both ctl and cKO mice exhibited similar motor activities shown by the speed and distance analysis. (*ctl=10, cKO=14, unpaired t-tests).*

Supplementary Figure legends

Supplementary Fig.1. OPC and oligodendrocyte density is not altered in the corpus callosum of mutant mice. a, Scheme of experimental schedule (left panel) and analyzed brain region in highlight, i.e. corpus callosum (cc, right panel). **b,** Corpus callosal OPCs and oligodendrocytes of ctl and cKO mice were immunolabeled with PDGFRα and CC1 respectively at the age of 2w and 9w. Olig2 was used as lineage marker and tdTomato was indicator of recombined cells. **c,** OPC recombination efficiency in ctl and cKO cc (ctl=86.22±0.57 (n=3), cKO=76.17±3.10 (n=6), unpaired t-test). **d, e,** Cell density of OPCs (PDGFRα$^+$) and oligodendrocytes (CC1$^+$) in cc of 2w- and 9w-old mice were not changed. OPC: (2w-ctl=77.02±4.21 (n=8), 2w-cKO=80±4.72 (n=8), unpaired t-test) (9w-ctl=30.01±3.68 (n=4), 9w-cKO=27.56±2.26 (n=4), unpaired t-test); oligodendrocytes (2w-ctl=121.70±12.31 (n=8), 2w-cKO=97.62±10.54 (n=8), unpaired t-test) (9w-ctl=296.90±32.83 (n=4), 9w-cKO=300.30±28.47 (n=4), unpaired t-test). **f,** Percentage of oligodendrocytes among total Olig2$^+$ cell population, considered as OPC differentiation rate, was not changed at both ages (2w-ctl=60.26±3.61(n=8), 2w-cKO=53.98±3.73 (n=8), unpaired t-test) (9w-ctl=92.37±0.12 (n=3), 9w-cKO=91.33±0.69 (n=6), unpaired t-test).

Supplementary Fig.2. Parameters of myelination remain largely unaltered in the corpus callosum of mutant mice. a, Scheme of experimental schedule (left panel) and analyzed brain region in highlight, i.e. mPFC and cc. **b,** Quantification of node length of ctl and cKO mPFC. **c,** Paranode length is increased in the cKO mPFC. **d,** Density of nodes remained same in the cKO mPFC. **e,** Relative mRNA level of MBP is reduced in the cKO mPFC, while PLP mRNA is not affected (ctl: n=4, cKO: n=3, unpaired t-test). **f,** Immunostaining of Caspr and MBP in cc of ctl and cKO mice. **g-i,** Paranodal length and node density in ctl and cKO cc remained same. **j,** Electron microscopic analysis of myelin ultrastructure in sagittal section of cc from ctl and cKO

mice. **k, l,** Quantification of g-ratios of axonal myelination shows unchanged myelination in cKO cc. **m,** Compound action potential conduction velocity was not altered indicated by patch clamp recordings. N1 indicates non-myelinated axonal conduction velocity, while N2 is for myelinated axons.

Supplementary Fig.3. Ablation of $GABA_BR$ in oligodendrocytes do not affect formation and density of oligodendrocytes. a, Scheme of transgene construction. **b,** Experimental schedule. **c,** Overview of CC1 immunostaining in a sagittal section of 9w old ctl mouse. Extensive tdTomato distribution shows a high recombination in different brain regions of transgenic mouse. **d,** Magnified images from prefrontal cortex (yellow box in **c**) and corpus callosum (white box in **c**). **e,** Quantification of oligodendrocyte recombination efficiency in PFC were identical, while cKO mice showed smaller recombination efficiency in cc. However, density of oligodendrocyte cells did not differ between ctl and cKO mice in both PFC and cc. arrows: recombined oligodendrocyte; triangles: non-recombined oligodendrocyte.

Supplementary Fig.4. Dense population of parvalbumin-expressing interneurons in the adult mouse cortex. a, Overview of coronal brain slices immunostained with parvalbumin and MBP shows abundant PV^+ neurons in the somatosensory cortex. **b,** Magnified view (yellow box in **a**) shows the absence of PV^+ axons in the corpus callosum.

Supplementary Fig.5. At the onset of myelination, $GABA_BR$-deficient OPCs receive less GABAergic input in the mPFC mutant mice. a, Experimental timeline and analyzed brain region (mPFC) in highlight.**b,** Immunostaining of PDGFRα and vGAT in the mPFC of p10 mice. **c,** Quantitative analysis of vGAT volume and the distance to OPC surface (ctl: n=4, cKO: n=4). **d,** The volume of vGAT in cKO mPFC was smaller than that in ctl group.

Supplementary Fig.6. The differentiation of $GABA_BR$-deficient OPCs is suppressed in the mutant mPFC. a, Scheme of experimental schedule and analyzed brain region (mPFC). **b,** Recombination efficiency of OPCs (% of $PDGFR\alpha^+tdt^+/PDGFR\alpha^+$) at p14 is identical in the ctl and cKO mPFC. **c,** Immunostaining and quantification of OPCs incorporated with BrdU shows no change in OPC proliferation in the cKO mPFC at p14 (*ctl: n=4, cKO: n=5, unpaired t-test*). **d,** Immunostaining and quantification of oligodendrocytes incorporated with BrdU shows decreased OPC differentiation in the cKO mPFC at p14 (*ctl: n=4, cKO: n=5, unpaired t-test*). **e,** The portion of oligodendrocytes among the oligodendrocyte lineage declined in cKO mPFC at p14 (*ctl: n=5, cKO: n=4, unpaired t-test*).

Supplementary Fig.7. Controlled ablation of $GABA_BR$ in OPCs of young adult mice does not affect oligodendrogenesis. a, Scheme of experimental schedule and the analyzed brain regions (mPFC and cc). **b,** Immunostaining of OPCs (PDGFRα) and oligodendrocyte (CC1) with Olig2 (lineage marker) at ctl and cKO mouse mPFC and cc at the age of 9w. **c, d,** Cell densities of OPCs ($PDGFR\alpha^+$) and oligodendrocytes ($CC1^+$) of cKO animals were the same as those for ctl mice in both mPFC and cc. mPFC: *($PDGFR\alpha^+$: (ctl=17.58±0.53 (n=4), cKO=18.69±1.58 (n=2), unpaired t-test)) ($CC1^+$: (ctl=9.05±1.38 (n=4), cKO=7.95±1.40 (n=2), unpaired t-test));* cc: *($PDGFR\alpha^+$: (ctl=35.38±2.25 (n=4), cKO=32.37±4.81 (n=2), unpaired t-test)) ($CC1^+$: (ctl=311.81±43.39 (n=4), cKO=339.20±70.53 (n=2), unpaired t-test))*. **e,** the Proportion of oligodendrocyte among total lineage cells did not change, suggesting OPC differentiation remained same in the mutant mouse mPFC and cc. mPFC: *(ctl=30.49±5.13 (n=3), cKO=29.91±2.62 (n=2), unpaired t-test); cc: (ctl=89.52±1.30 (n=3), cKO=91.21±0.471 (n=2), unpaired t-test)*.**f,** MBP expression is not altered in the cKO mPFC at mRNA level. (ctl: n=4, cKO: n=3, unpaired t-test).

Supplementary Fig.8. The apoptosis of interneurons is mitigated in the mPFC of mutant mice at p14. a, Timeline of experiments and scheme of analyzed brain

region mPFC in highlight. **b,** Immunostaining of PV^+ neurons with apoptotic marker (cleaved caspase-3) at p10 of ctl and cKO mPFC. **c,** Quantification of apoptotic PV^+ neurons at p10 and p14 shows reduced PV^+ neuronal apoptosis in the cKO mPFC compared to ctl (p10*: ctl=2.03±0.47 (n=6), cKO=0.92±0.34 (n=3), unpaired t-test;* p14: *ctl=3.70±1.21 (n=6), cKO=2.50±0.72 (n=9), unpaired t-test)*. **d,** Representative images of apoptotic neurons at p14 of ctl and cKO mPFC. **e,** Quantification of apoptotic total neurons ($NeuN^+CC\text{-}3^+$) at p14 *(ctl=2.76±0.42 (n=12), cKO=1.42±0.29 (n=9), unpaired t-test)*.

Supplementary Fig.9. Ablation of $GABA_BR$ expression in OPCs does not affect the apoptosis or survival of excitatory neurons. a, Scheme of experimental schedule (left panel) and analyzed brain region in highlight. **b,** About 40 % of OPCs are recombined (% of $PDGFR\alpha^+tdT^+/PDGFR\alpha^+$) at p7 both in the ctl and cKO mPFC. **c, d,** Immunostainings and quantification of excitatory neurons ($TBR1^+$) with apoptotic marker CC-3 in mPFC of ctl and cKO pups at p5 (**c**) and p7 (**d**) (p5: *ctl=1.64±0.39 (n=4), cKO=1.74±0.24 (n=4), unpaired t-test;* p10*: ctl=0.74±0.18 (n=4), cKO=0.67±0.16 (n=4), unpaired t-test*).

Supplementary Fig.10. TWEAK expression in OPCs is regulated by $GABA_BRs$. a, Scheme of experimental design. **b,** Relative mRNA level of cytokines in the mPFC of ctl and cKO mouse at p7 *(TNF-α: ctl=1±0.34 (n=4), cKO=1.23±0.36 (n=6), unpaired t-test) (TWEAK: ctl=1±0.10 (n=4), cKO=0.67±0.08 (n=6), unpaired t-test) (FasL: ctl=1±0.57 (n=2), cKO=0.91±0.23 (n=4), unpaired t-test) (TNFSF7: ctl=1±1.00 (n=4), cKO=0.93±0.67 (n=6), unpaired t-test) (Trp53: ctl=1±0.11 (n=4), cKO=1.14±0.08 (n=6), unpaired t-test) (NGF: ctl=1±0.24 (n=5), cKO=1.08±0.18 (n=6), unpaired t-test)*. **c,** Western blot analysis of TWEAK expression in Oli-neu cells treated with 50 μM Baclofen at the presence or absence of 20 μM CGP 55845 (n=5 independent experiments). The isoform in 36 KDa (blue box) was analyzed.

Supplementary Fig.11. OPC-GABA$_B$R cKO mice exhibit impaired social behavior. a, b, Mutant mice stayed longer at the chamber of mouse than object, indicating that sociability of the mutant mouse is not affected. **c, d,** Mutant mice spent similar time at the chambers of familiar and unfamiliar mouse, suggesting impaired cognition of the cKO mice (ctl (n=9), cKO (n=9), paired t-test).

Figure 1

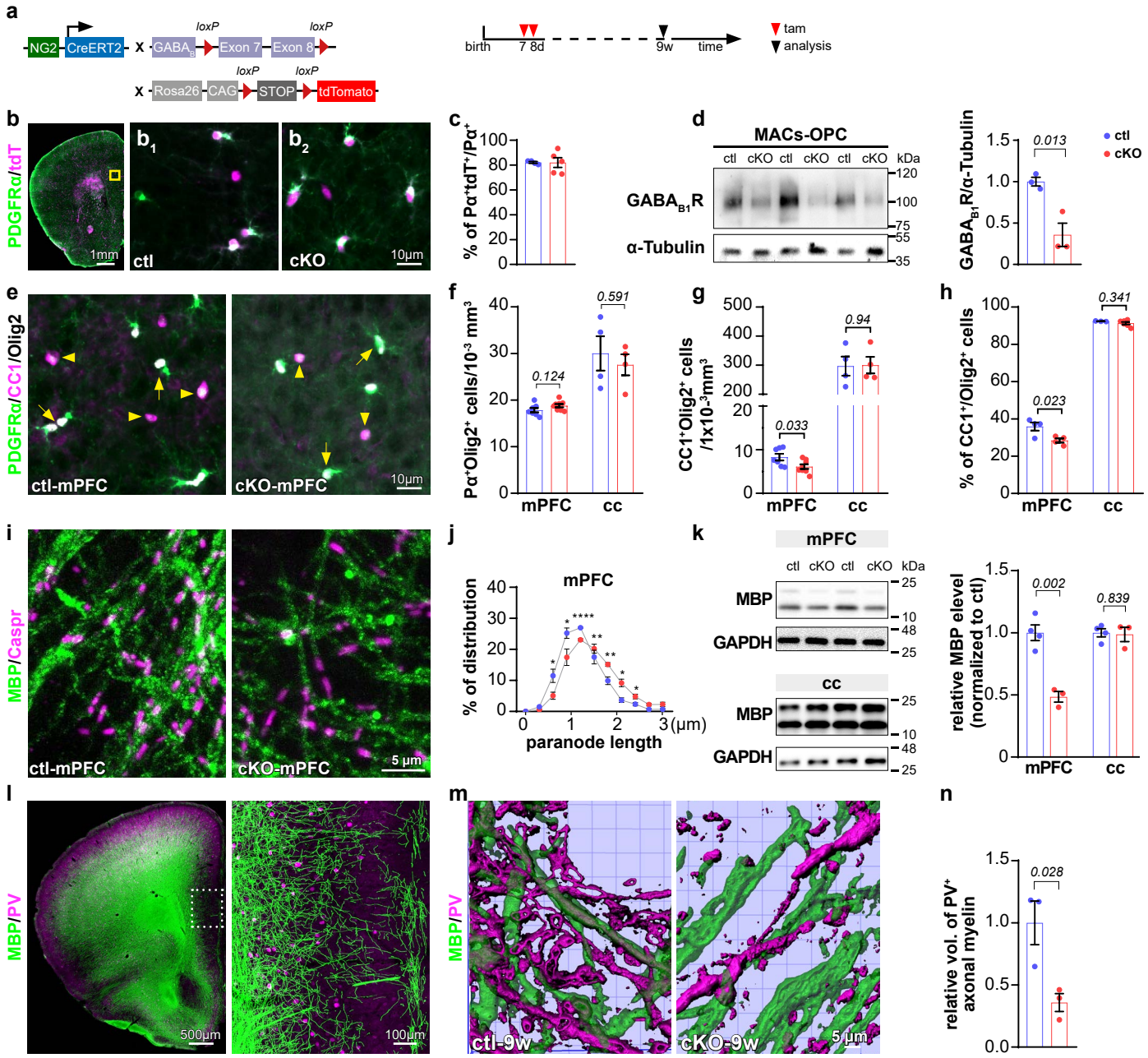
a
NG2
CreERT2
GABA
loxP
Exon 7
Exon 8
Rosa26
CAG
STOP
tdTomato
birth
7 8d
9w
time
tam
analysis
b
PDGFRα/tdT
1mm
ctl
cKO
10μm
c
% of Pα+tdT+/Pα+
d
MACs-OPC
ctl cKO ctl cKO ctl cKO
kDa
GABAB1R
α-Tubulin
GABAB1R/α-Tubulin
0.013
e
PDGFRα/CC1/Olig2
ctl-mPFC
cKO-mPFC
f
Pα+Olig2+ cells/10-3 mm3
0.124
0.591
mPFC
cc
g
CC1+Olig2+ cells /1x10-3mm3
0.033
0.94
h
% of CC1+/Olig2+ cells
0.023
0.341
i
MBP/Caspr
5 μm
j
mPFC
% of distribution
paranode length
k
MBP
GAPDH
relative MBP elevel (normalized to ctl)
0.002
0.839
l
MBP/PV
500μm
100μm
m
ctl-9w
cKO-9w
n
relative vol. of PV+ axonal myelin
0.028

Figure 2

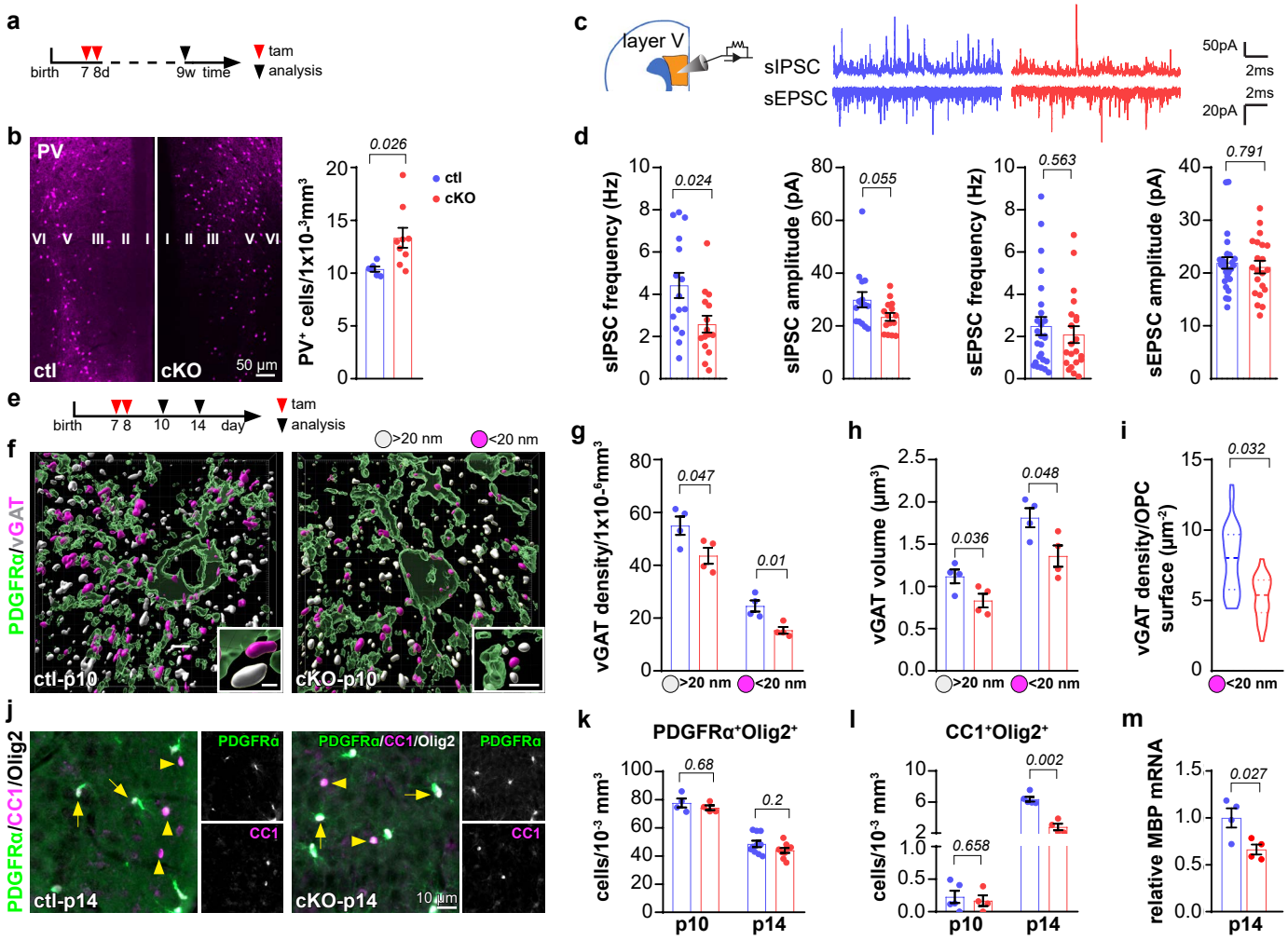
a
birth
7 8d
9w time
tam
analysis
b
PV
VI V III II I
I II III V VI
ctl
cKO
50 µm
PV⁺ cells/1x10-3mm3
0.026
ctl
cKO
c
layer V
sIPSC
sEPSC
50pA
2ms
2ms
20pA
d
sIPSC frequency (Hz)
0.024
sIPSC amplitude (pA)
0.055
sEPSC frequency (Hz)
0.563
sEPSC amplitude (pA)
0.791
e
birth
7 8
10
14
day
tam
analysis
f
PDGFRα/vGAT
>20 nm
<20 nm
ctl-p10
cKO-p10
g
vGAT density/1x10-6mm3
0.047
0.01
>20 nm
<20 nm
h
vGAT volume (µm3)
0.036
0.048
>20 nm
<20 nm
i
vGAT density/OPC surface (µm-2)
0.032
<20 nm
j
PDGFRα/CC1/Olig2
PDGFRα
CC1
PDGFRα/CC1/Olig2
PDGFRα
CC1
ctl-p14
cKO-p14
10 µm
k
PDGFRα⁺Olig2⁺
cells/10-3 mm3
0.68
0.2
p10
p14
l
CC1⁺Olig2⁺
cells/10-3 mm3
0.658
0.002
p10
p14
m
relative MBP mRNA
0.027
p14

Figure 3

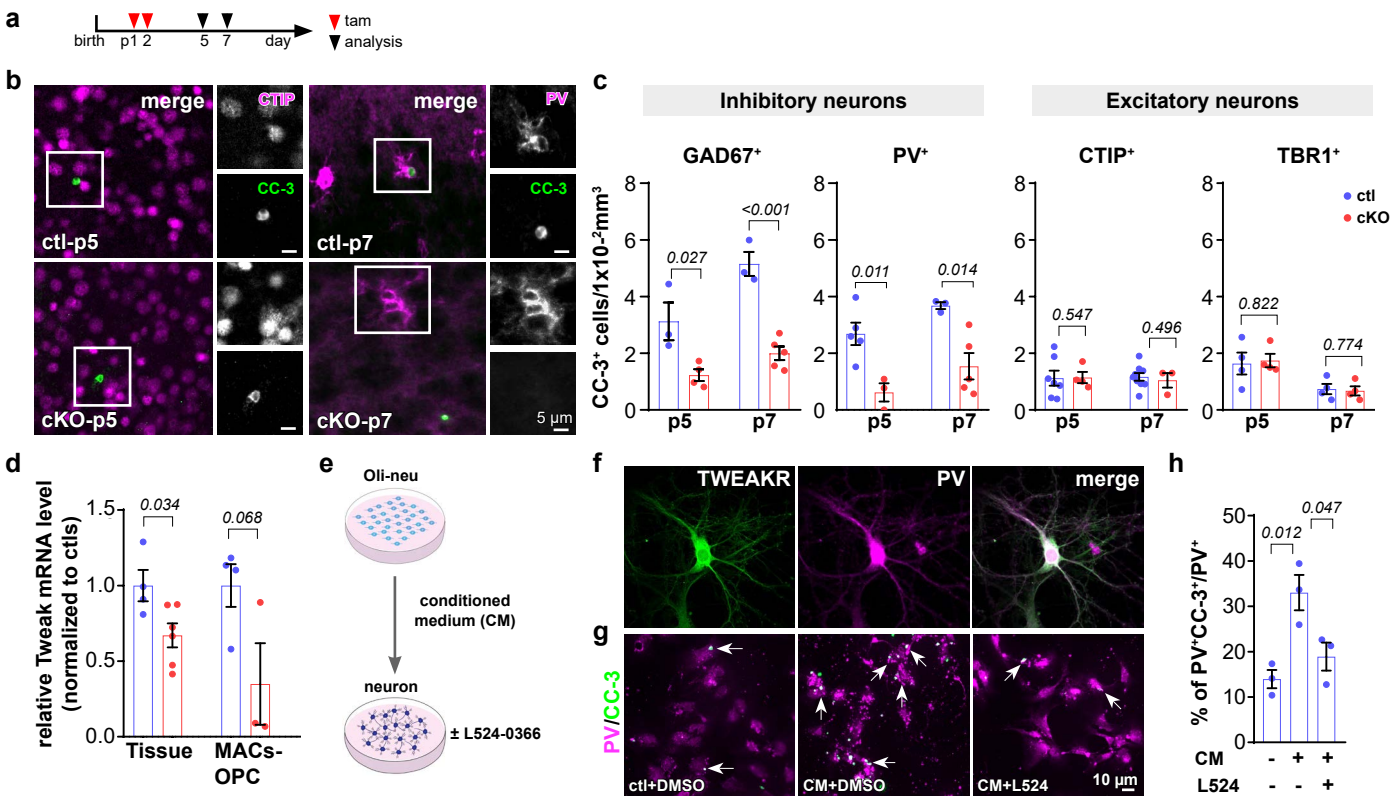
a
birth
p1 2
5
7
day
tam
analysis
b
merge
CTIP
CC-3
ctl-p5
cKO-p5
merge
PV
CC-3
ctl-p7
cKO-p7
5 µm
c
Inhibitory neurons
Excitatory neurons
GAD67+
PV+
CTIP+
TBR1+
CC-3+ cells/1x10-2mm3
0.027
<0.001
0.011
0.014
0.547
0.496
0.822
0.774
p5
p7
ctl
cKO
d
relative Tweak mRNA level (normalized to ctls)
0.034
0.068
Tissue
MACs-OPC
e
Oli-neu
conditioned medium (CM)
neuron
± L524-0366
f
TWEAKR
PV
merge
g
PV/CC-3
ctl+DMSO
CM+DMSO
CM+L524
10 µm
h
% of PV+CC-3+/PV+
0.012
0.047
CM
L524

Figure 4

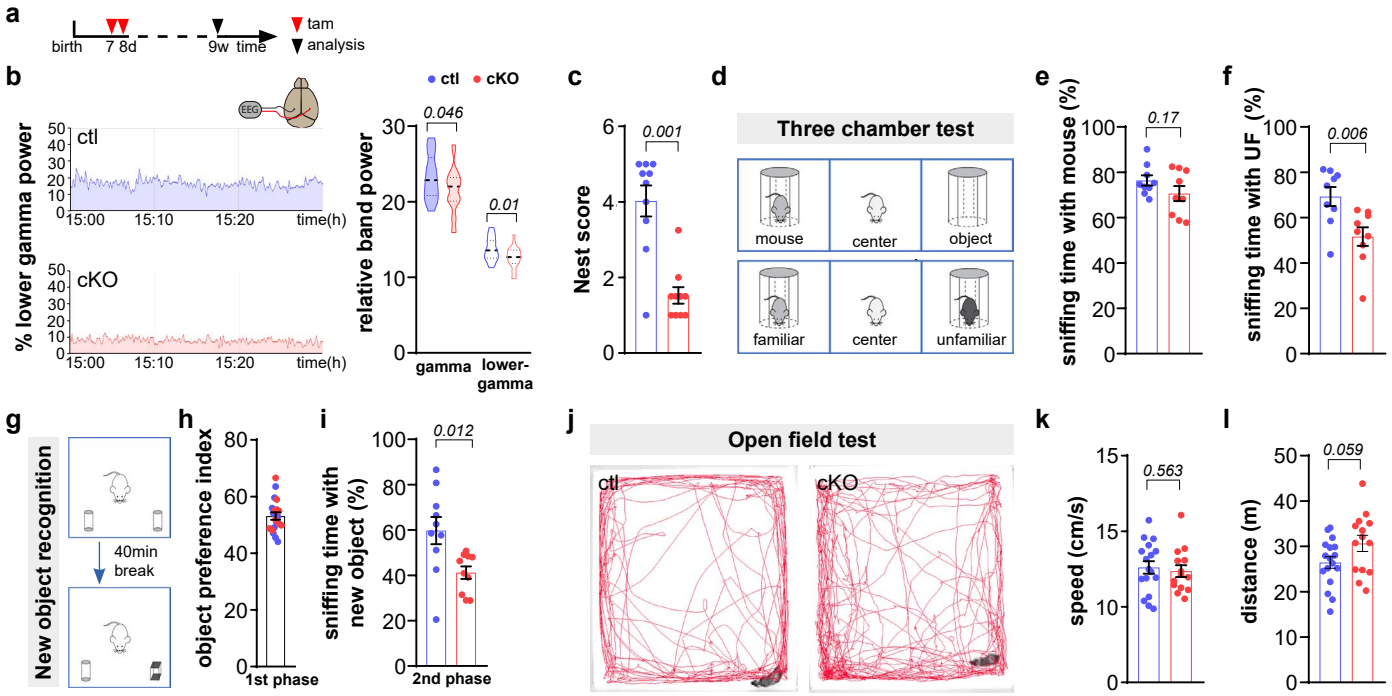
a
birth
7 8d
9w
time
tam
analysis
b
EEG
ctl
cKO
% lower gamma power
15:00
15:10
15:20
time(h)
relative band power
0.046
0.01
gamma
lower-gamma
c
Nest score
0.001
d
Three chamber test
mouse
center
object
familiar
center
unfamiliar
e
sniffing time with mouse (%)
0.17
f
sniffing time with UF (%)
0.006
g
New object recognition
40min
break
h
object preference index
1st phase
i
sniffing time with new object (%)
0.012
2nd phase
j
Open field test
ctl
cKO
k
speed (cm/s)
0.563
l
distance (m)
0.059

Supplementary figure 1

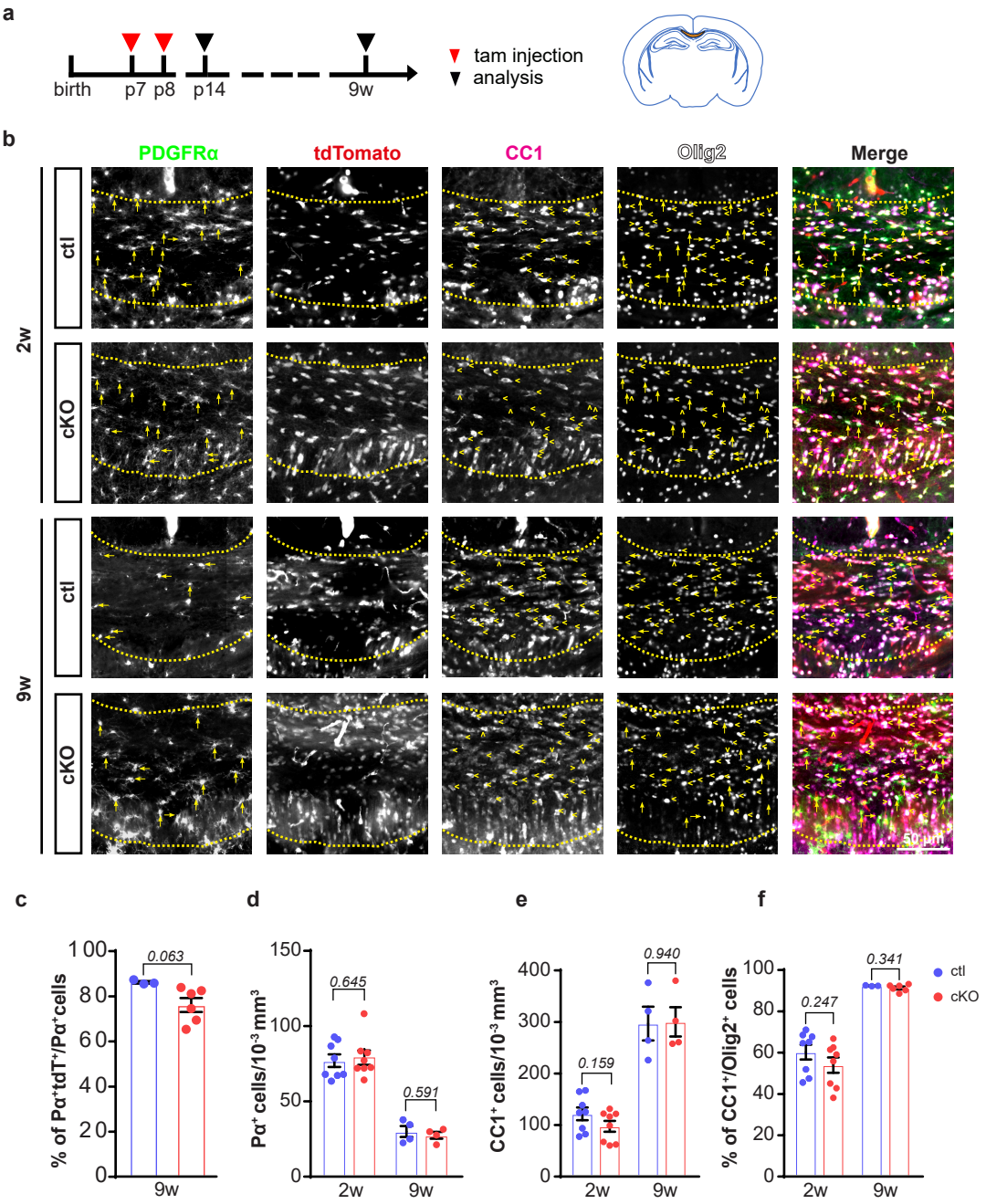

Supplementary figure 2

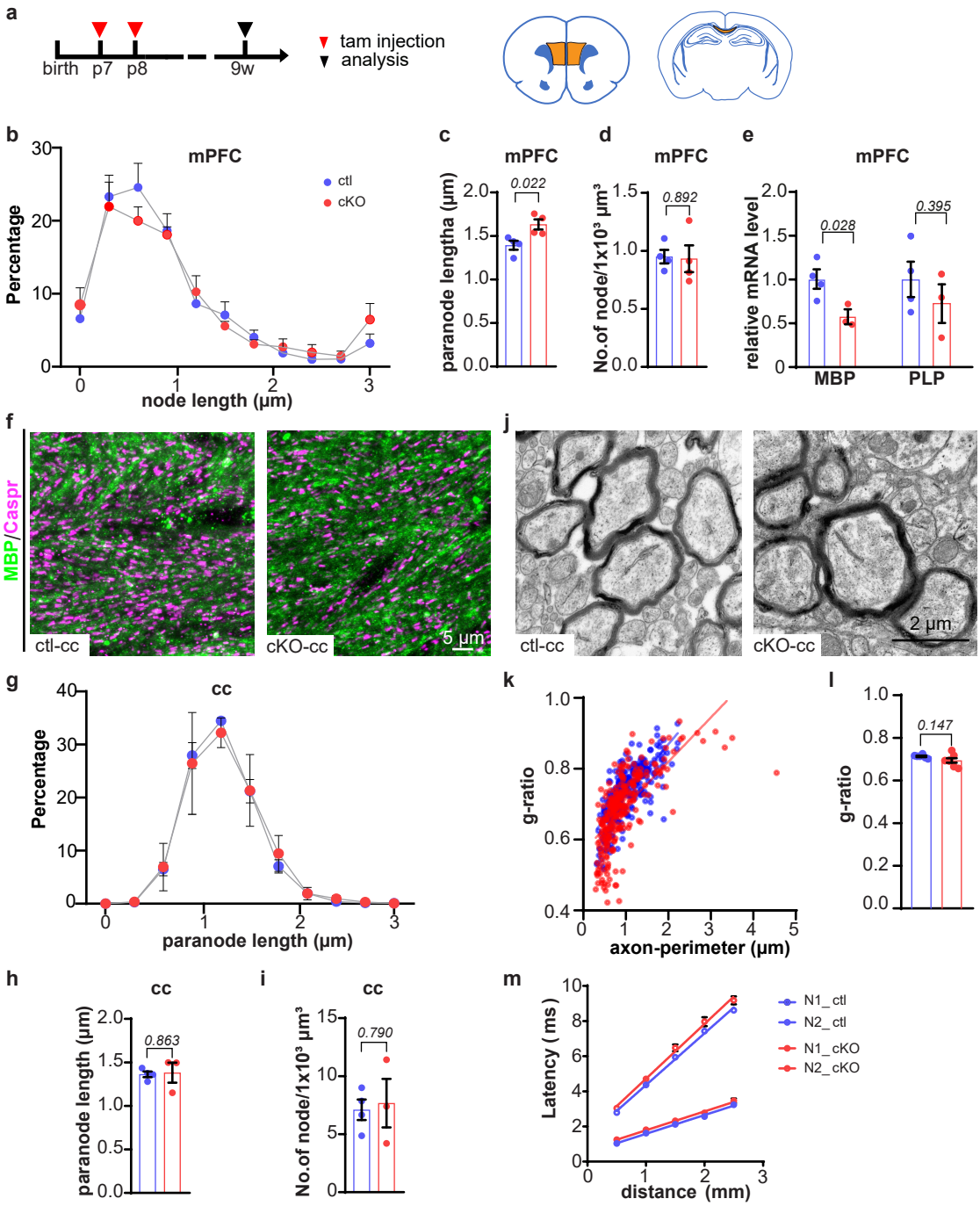

Supplementary figure 3

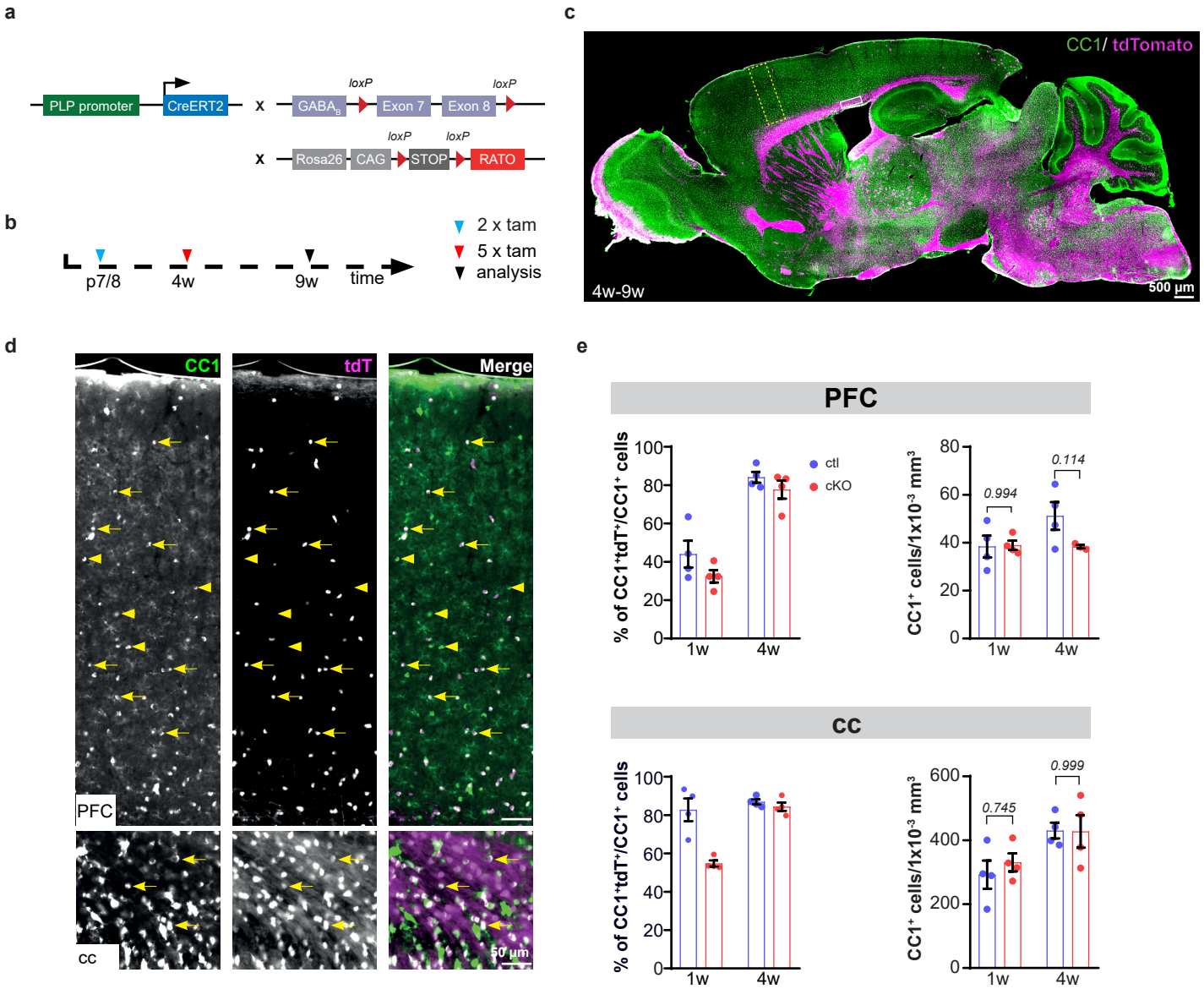

Supplementary figure 4

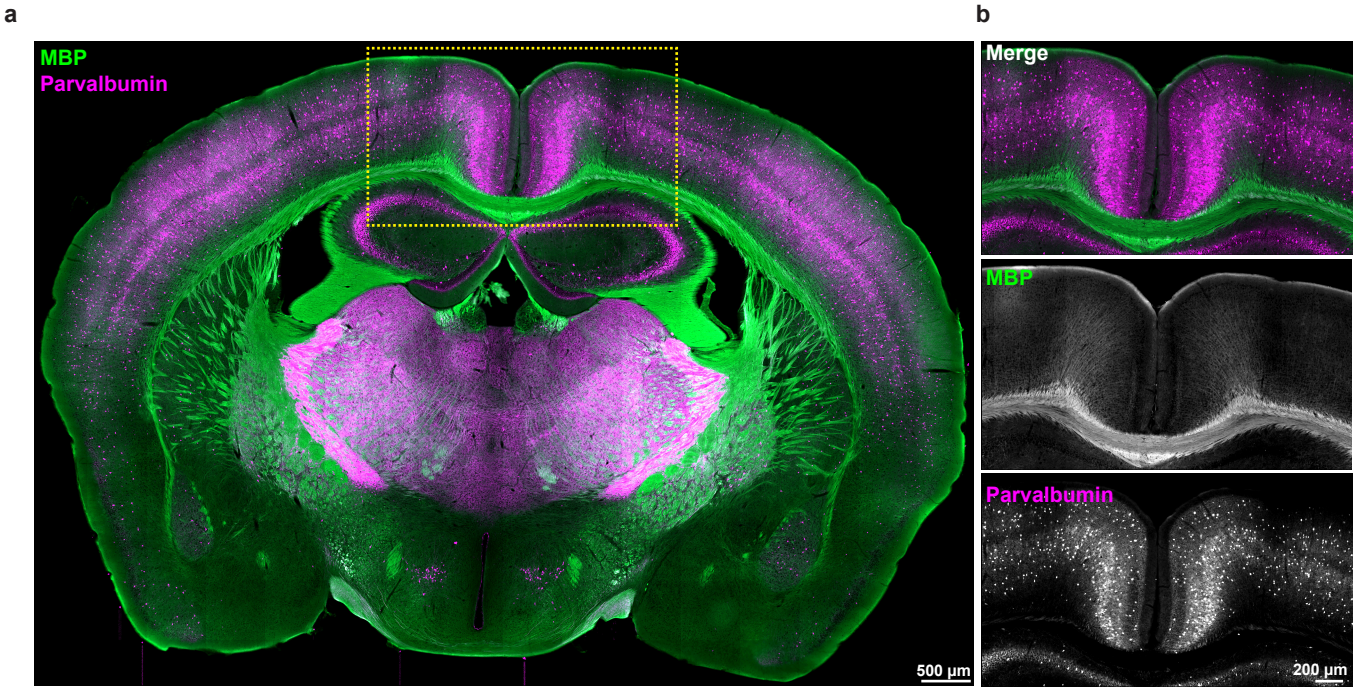

Supplementary figure 5

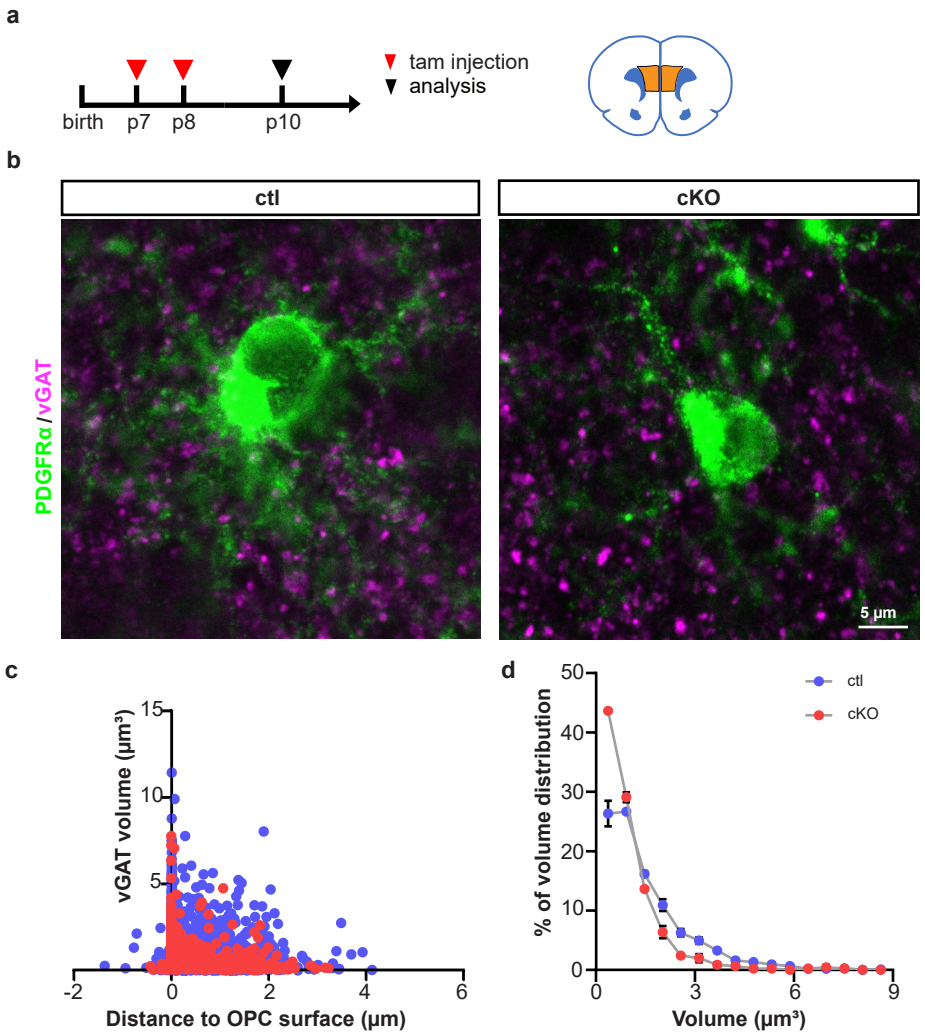

Supplementary figure 6

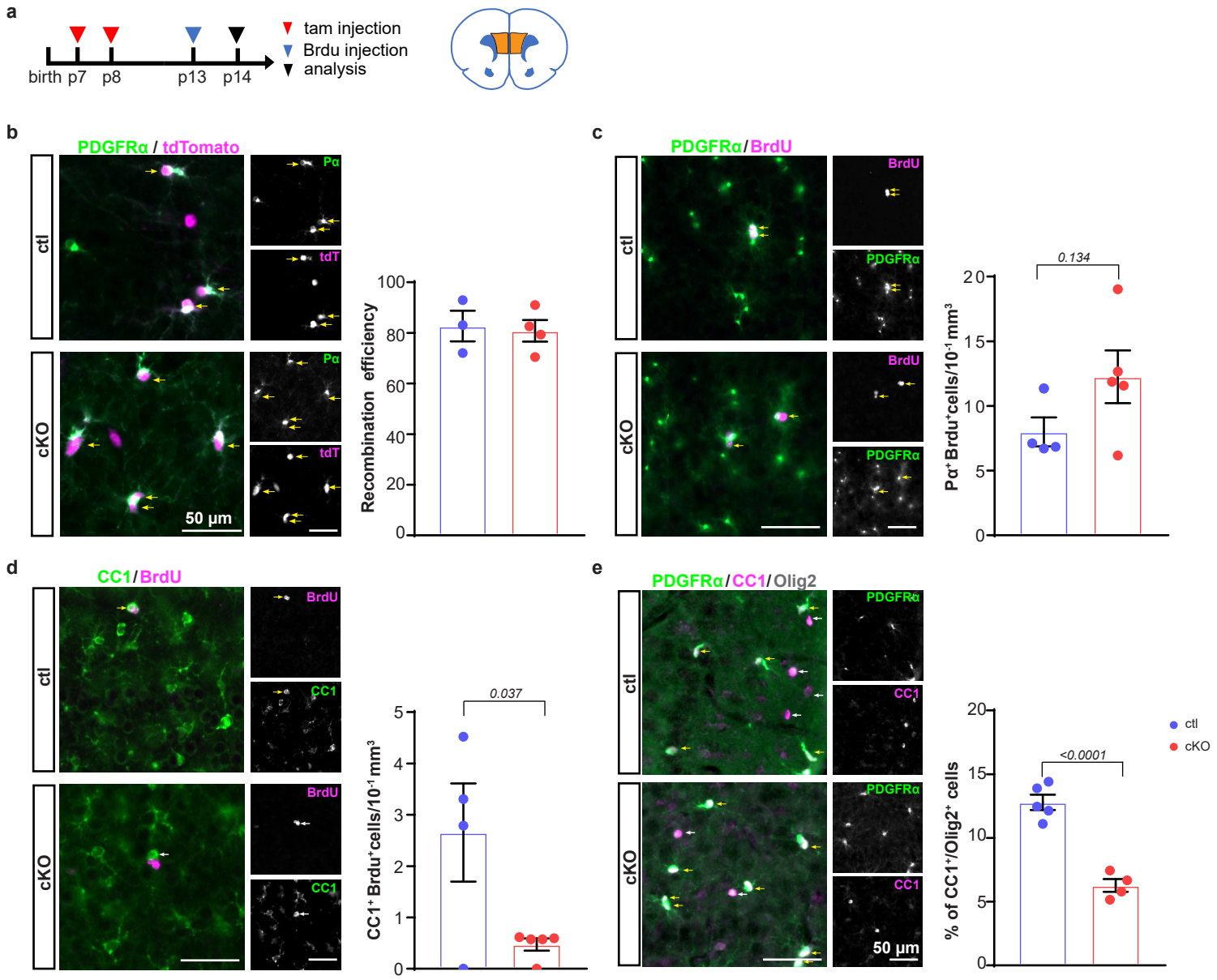

Supplementary figure 7

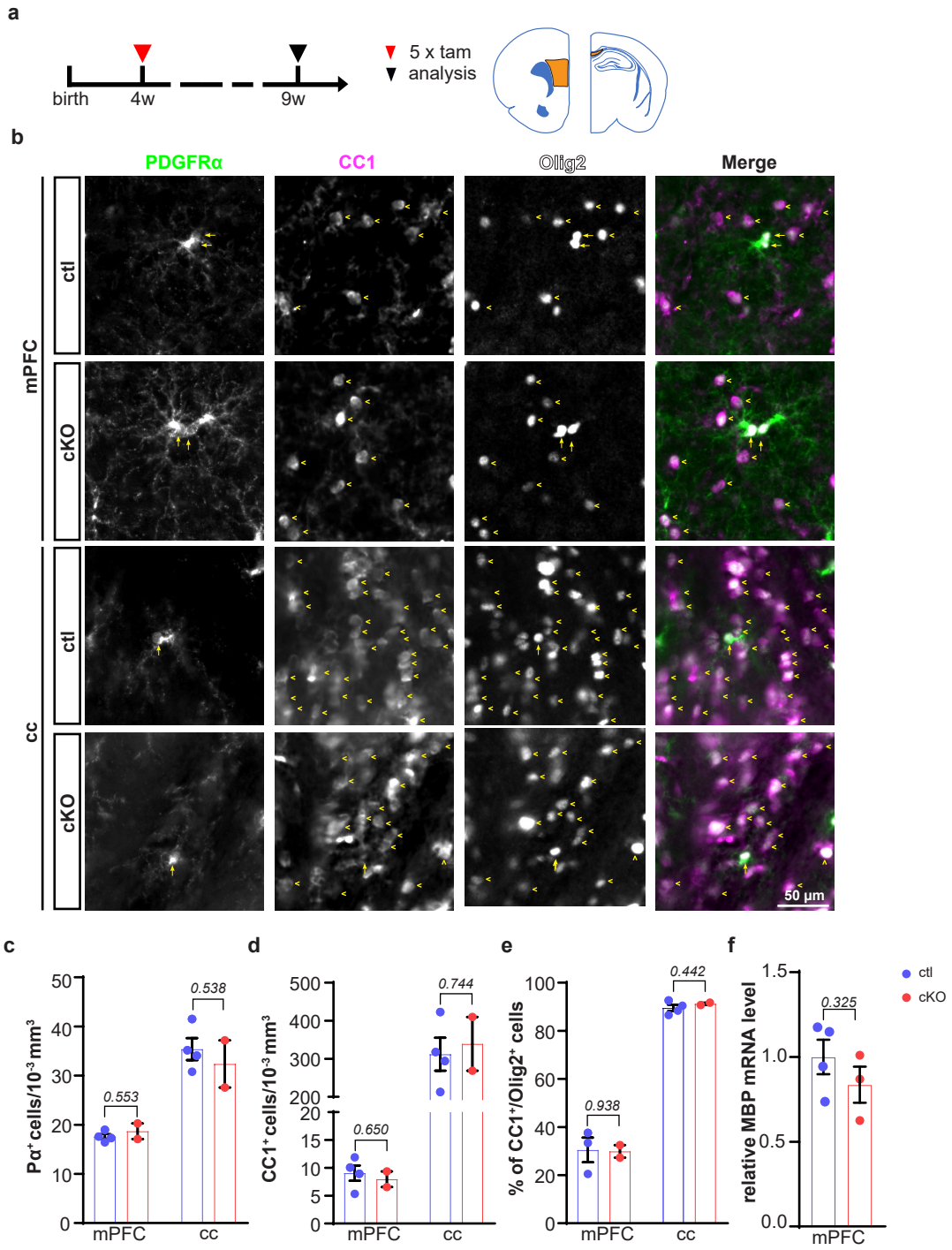

Supplementary figure 8

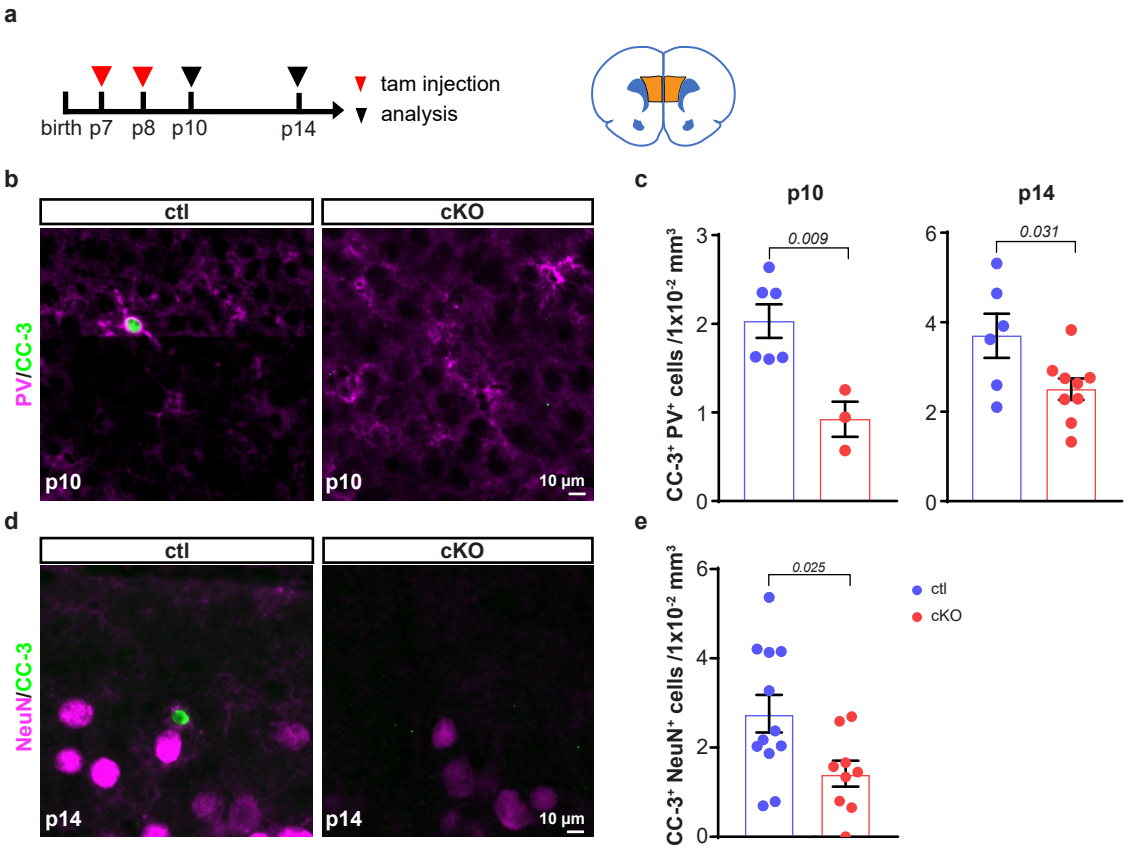

Supplementary figure 9

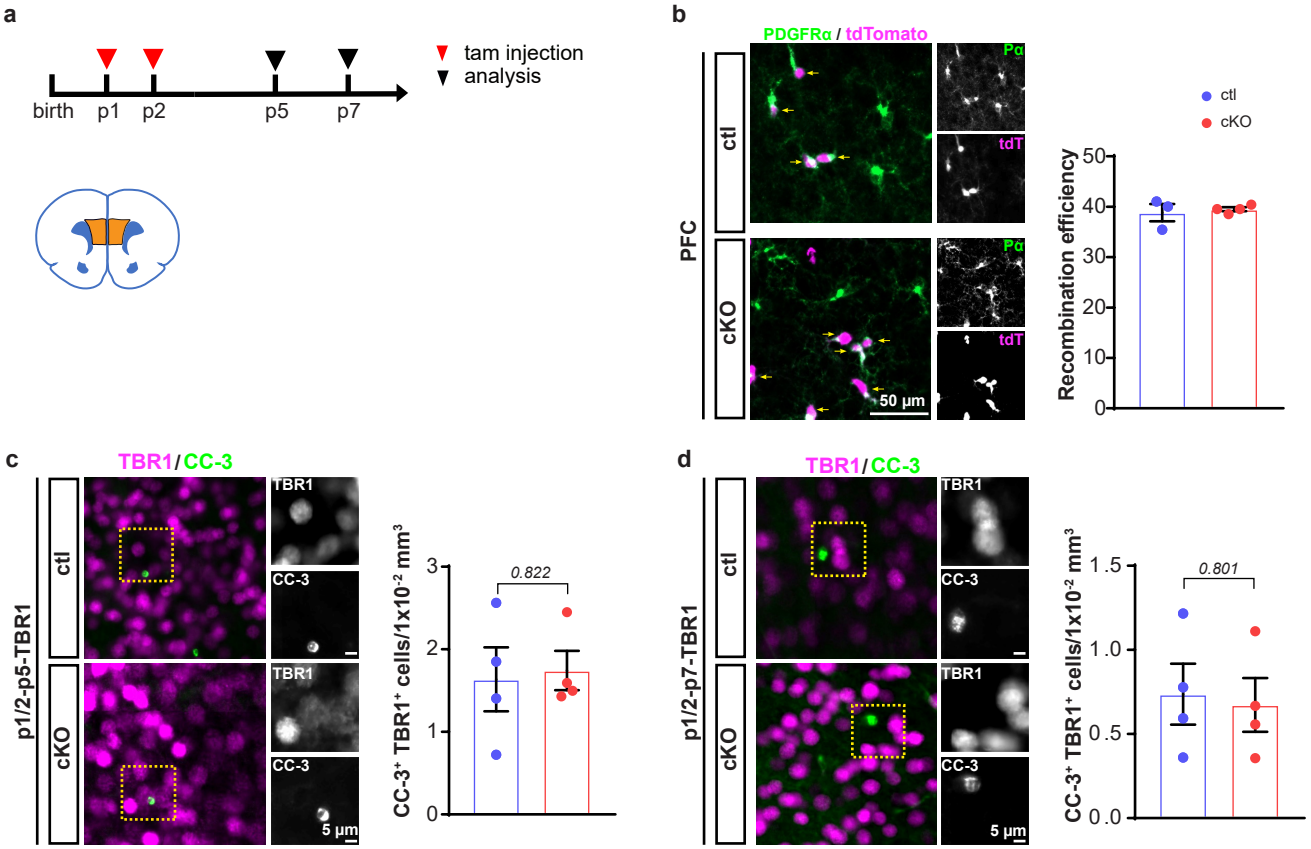

Supplementary figure 10

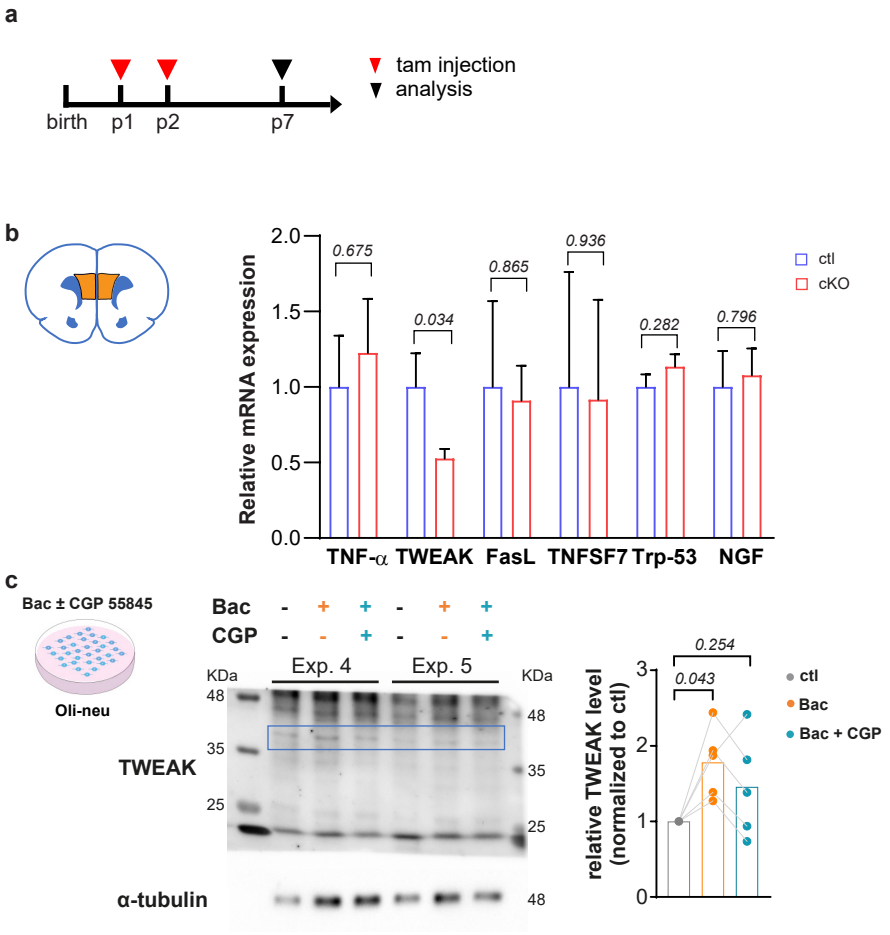
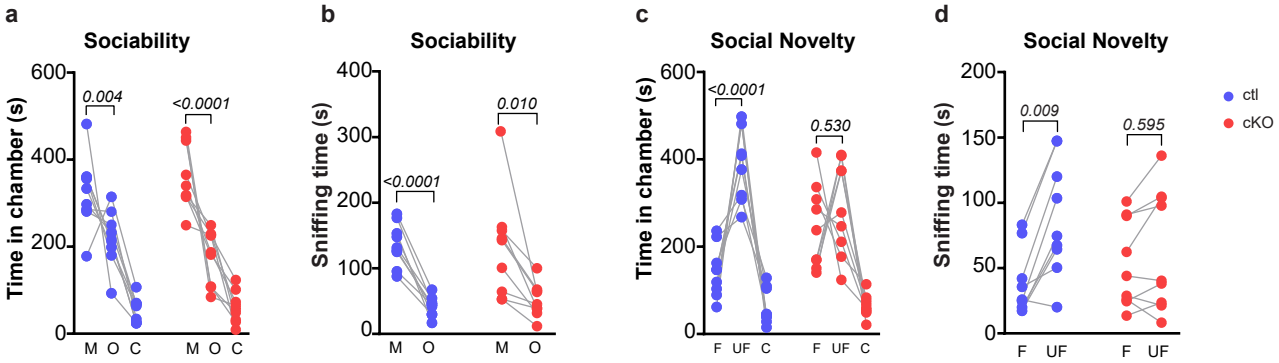
Supplementary figure 11